Journal of Hydrology 668 (2026) 134959

Contents lists available at ScienceDirect

Journal of Hydrology

journal homepage: www.elsevier.com/locate/jhydrol

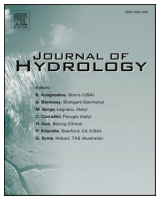

Research papers

Robustness of critical soil moisture to curve-fitting methods and its variability with soil depth, soil texture, and climatic conditions: insights from lysimeter data in Germany

Xiao Lu [a,b,i,*], Jannis Groh [a,c,d], Alexander Graf [a], Thomas Pütz [a], Horst H. Gerke [e], Ralf Gründling [f], Holger Rupp [f], Ralf Kiese [g], Hans Jörg Vogel [f], Mathieu Javaux [a,h], Harry Vereecken [a], Harrie-Jan Hendricks Franssen [a]

[a] Institute of Bio- and Geoscience IBG-3: Agrosphere, Forschungszentrum Jülich GmbH, Jülich, Germany
[b] Faculty of Georesources and Materials Engineering, RWTH Aachen University, Aachen, Germany
[c] Department of Soil Science and Soil Ecology, University of Bonn, Institute of Crop Science and Resource Conservation, Bonn, Germany
[d] Research Area 1 "Landscape Functioning", Working Group "Isotope Biogeochemistry and Gas Fluxes", Leibniz Centre for Agricultural Landscape Research (ZALF), Müncheberg, Germany
[e] Research Area 1 "Landscape Functioning", Working Group "Agricultural Biogeochemistry", Leibniz Centre for Agricultural Landscape Research (ZALF), Müncheberg, Germany
[f] Department of Soil System Science, Helmholtz-Centre for Environmental Research – UFZ, Halle, Saale, Germany
[g] Karlsruhe Institute of Technology, Institute for Meteorology and Climate Research, Atmospheric Environmental Research (IMK-IFU), Garmisch-Partenkirchen, Germany
[h] Earth and Life Institute, Environmental Sciences, UCLouvain, Belgium
[i] Water, Energy and Environmental Engineering Research Unit, University of Oulu, Finland

ARTICLE INFO

This manuscript was handled by Marco Borga, Editor-in-Chief, with the assistance of Christian Massari, Associate Editor

Keywords:
Evapotranspiration
Critical soil moisture threshold
Weighable lysimeter
Root zone soil moisture
Changing climatic conditions
Curve fitting

ABSTRACT

Actual evapotranspiration (ET_a) is a vital terrestrial ecosystem process that links water, energy, and carbon cycles. ET_a can be limited by either energy or water availability. The transition between water- and energy-limited regimes is related to soil moisture and is often characterized as a threshold, denoted as critical soil moisture threshold (θ_{crit}). However, the determination of θ_{crit} is subject to uncertainties due to the different methods used to evaluate the relationship between ET_a and soil moisture (SM), such as SM depths, definitions of ET_a and curve fitting functions. Typically, surface SM is used to identify θ_{crit} as it is easily accessible and assumed to represent root zone SM status. Weighable lysimeter technology provides a unique opportunity to assess the role of root zone SM on the transition between water and energy limited ET_a. It is widely regarded as the gold standard for measuring in-situ ET, and at the same time allows for in-situ SM measurements at different depths. In this study, we estimated θ_{crit} using *in situ* SM measurements at 10 cm depth and root zone SM by vertically integrating *in situ* SM (0–60 cm) observations. In addition, we applied three different definitions of relative evapotranspiration (evaporative fraction, the ratio of ET_a to grass reference evapotranspiration and the ratio of actual ET_a to calculated potential evapotranspiration) as well as two different fitting curves to investigate the sensitivities of θ_{crit}. We found robust θ_{crit} estimates across different definitions and fitting curve methods, but the estimates were significantly higher for root zone than for surface θ_{crit}. Our results also highlight the high correlation (0.83) between root zone and surface θ_{crit}. However, the relation between both values is not unique since it depends on the actual moisture profile and plant root system and, herewith, on the soil type and previous weather conditions. We further observed that both surface and root zone θ_{crit} decreased with increasing sand fraction. Under changing climatic conditions but with identical soil and ecosystem types, both surface and root zone θ_{crit} decreased with increasing aridity. Additionally, we found that using the midpoint between field capacity and wilting point provides a reliable range of root zone θ_{crit} for a given soil texture.

* Corresponding author at: Institute of Bio- and Geoscience IBG-3: Agrosphere, Forschungszentrum Jülich GmbH, Jülich, Germany.
E-mail address: xi.lu@extern.fz-juelich.de (X. Lu).

https://doi.org/10.1016/j.jhydrol.2026.134959
Received 27 December 2024; Received in revised form 9 November 2025; Accepted 11 January 2026
Available online 13 January 2026

1. Introduction

Actual evapotranspiration (ET_a), as an essential component of the water, energy and carbon cycle, serves as a vital link between the land surface hydrological processes and atmospheric processes (Wang & Dickinson, 2012; Fisher et al., 2017; Corami et al., 2024). Two distinct ET_a regimes have earlier been recognized: a water-limited and an energy-limited regime (Budyko, 1974). The transition between the two regimes is associated with the soil moisture (SM) and occurs at or around a threshold value, denoted as critical soil moisture threshold (θ_{crit}; Seneviratne et al., 2010). When SM dries below θ_{crit}, ET_a falls into the water-limited regime, where plants experience water stress and ET_a is controlled by water availability. The reduction in SM causes plants to constrict the stomatal apertures to impede large leaf water potential drop and water losses, which decreases ET_a, thereby reducing evaporative cooling and increasing sensible heat flux from the land to the lower atmosphere (Koster et al., 2009; Humphrey et al., 2021). When SM is above θ_{crit}, in contrast, ET_a is mainly governed by energy supply; consequently, increased SM does not necessarily increase ET_a. In this energy-limited regime, stomatal aperture is no longer a constraint and thus ET_a reaches or approximates an upper limit bounded by atmospheric evaporative demand, commonly referred to as potential ET (PET; Xiang et al., 2020). Switching between the two regimes can potentially influence hydroclimatic extremes (e.g., floods, droughts, and heatwaves) by dampening or amplifying the land–atmosphere interactions (Berg et al., 2016; Zhang et al., 2020; Lo et al., 2021). Yet, a recent review revealed that the dependency of ET_a to SM is still badly represented in current land surface models (Green et al., 2024). Therefore, knowledge of θ_{crit} is crucial for better understanding the impacts of extreme weather events and improving land surface, hydrological and crop models to predict future climate and crop yields.

However, the quantification of θ_{crit} remains uncertain due to the lack of precise measurements on ET_a and SM. Based on the conceptual framework established by Budyko (1974) and Seneviratne et al. (2010), the most widespread determination of θ_{crit} is through the relationship between SM and a variable derived from ET_a (Fig. 1), such as evaporative fraction (EF; the ratio of latent heat flux to the available energy) representing the energy partitioning (Ford et al., 2014a), or evaporation factor (the ratio of ET_a to PET; hereafter rPET) describing the degree of water stress (Yao, 1974; Eagleson, 1978). Such a relationship is a function of soil and plant hydraulic, and stomatal control (Wankmüller et al., 2024). Moreover, θ_{crit} is a variable rather than a constant property as it is also a function of ET_a. Past efforts to evaluate θ_{crit} dominantly rely on model- and reanalysis-based data (Schwingshackl et al., 2017; Hsu and Dirmeyer, 2023a,b; Paul et al., 2025), remote sensing and satellite-based data (Feldman et al., 2019; Denissen et al., 2020; Dong et al., 2023; Koster et al., 2024), eddy covariance (EC) tower and *in situ* SM sensors (Haghighi et al., 2018; Dong et al., 2022; Fu et al., 2022), or a combination of these sources (Buitink et al., 2020; Fu et al., 2024; Liu et al., 2024). However, the model representation of the coupling between SM and ET_a is highly uncertain (Dirmeyer et al., 2000), and the results regarding ET_a sensitivity to SM depend strongly on the implemented assumption in the model concerning the relationship between SM and ET_a (Schwingshackl et al., 2017). On the other hand, remote sensing data, though promising, suffer from algorithmic uncertainties in ET_a estimates (Sörensson & Ruscica, 2018). Additionally, some products have pre-defined SM and evaporation relationships (Martens et al., 2017), potentially biasing the θ_{crit}. Therefore, a purely ground-based observation analysis would have certain advantages. However, while EC towers provide in-situ observations, they often do not close the energy balance and have changing footprint sizes and shapes (Franssen et al., 2010; De Kauwe et al., 2017). On top of that, the horizontal footprints of flux data vary from 100 m to few kilometers in radius around the towers (Chu et al., 2021; Zhu et al., 2023), whereas *in situ* SM sensors provide only point-scale measurements (Brown et al., 2023). The spatial variability of SM is influenced by heterogeneities in soil properties, vegetation, and topography within the flux footprint, which can pose a potential scale mismatch, leading to biases in θ_{crit} assessments (Iwema et al., 2017).

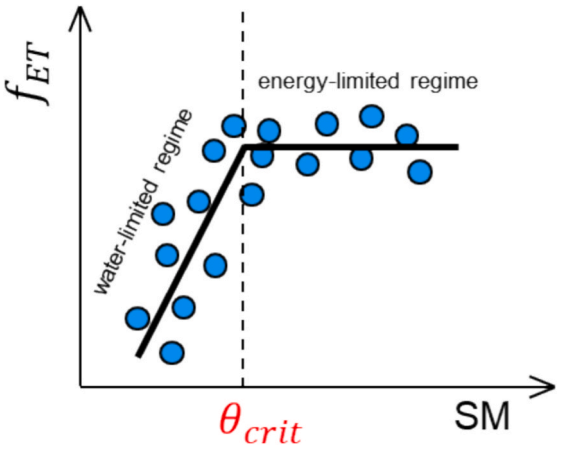

Fig. 1. Schematic plot showing the assessment of f_{ET}-SM relationship, where f_{ET} represents either EF, rET_0 or $rPET_{FAO}$. SM can be from soil surface (θ_s) or from the root zone (θ_v). Blue dots represent the data points during dry downs over the growing periods. The thick black line denotes the linear-plus-plateau fitting.

The next major challenge in understanding θ_{crit} lies in the impact of measurement depth on its estimation. Most previous studies focused primarily on surface SM (e.g., at a sampling depth of less than 5 cm for remote sensing, Escorihuela et al., 2010; Akbar et al., 2018; Feldman et al., 2019; Denissen et al., 2020; Fu et al., 2024) or root zone SM estimated from shallow surface SM due to the lack of deeper SM measurements (Koster et al., 2024). Few studies have explicitly compared θ_{crit} derived from both surface and root zone SM. However, plants can access water stored deeply in the soil to sustain transpiration (Oliveira et al., 2005; Thompson et al., 2011). Although some studies argued that surface SM and root zone SM are closely correlated (Ford et al., 2014b), thereby implying similar surface energy balance characteristics (Qiu et al., 2016, 2020; Dong et al., 2022; Paul et al., 2025), some studies presented contrasting conclusions. For example, Mahmood & Hubbard (2007) found the correlation and cross-correlation between surface SM and subsurface SM declines rapidly with increasing depth under various land use types, suggesting estimating root zone SM based on surface SM is problematic. Likewise, Hirschi et al. (2014) pointed out that the temporal dynamics of surface SM and root zone SM decouple gradually during extreme hot conditions. Recently, Buitink et al. (2020) reported a lower θ_{crit} value for surface soil compared to root zone soil. Hence, it remains questionable whether the θ_{crit} of the surface SM is consistent with that of the root zone SM.

Alternatively, weighable lysimeters are regarded as the best method to measure in situ ET_a (Schrader et al., 2013; Gebler et al., 2015; Lu et al., 2024), which are capable of measuring the complete water balance, avoiding the underestimation of ET_a due to the energy imbalance issue present in the EC approach. Many studies regarded lysimeter-based ET_a as a reference to address the energy balance closure problem and correct EC-based ET_a (Gebler et al., 2015; Hirschi et al., 2017; Widmoser & Wohlfahrt, 2018; Mauder et al., 2021). With SM sensors installed at several depths in the profile within the lysimeter, data pairs of SM and ET_a can be accurately obtained, providing a unique insight into the surface and root zone SM controls on ET_a. The German TERrestrial ENvironmental Observatories (TERENO) SOILCan network is such a lysimeter network, equipped with high-precision and high-resolution weighable lysimeters (Pütz et al., 2016; Kiese et al., 2018; Zacharias et al., 2024), offering the possibility to investigate surface and root zone θ_{crit} using precise lysimeter measurements.

As θ_{crit} is estimated from a fitting procedure based on a conceptual

framework (Fig. 1), its uncertainty can also arise from the definitions of relative ET_a (the y axis variable). As mentioned above, both EF and rPET can be used to estimate θ_{crit} using a linear-plus-plateau fit due to their same idealized structure curve as depicted in Fig. 1. However, to our knowledge, no previous studies have examined what the impact of the definitions of relative ET_a (EF versus rPET) is on estimating θ_{crit}, as existing studies have typically focused on only one definition of relative ET_a. Although the relationship between rPET and SM has been studied long ago (e.g., Manabe, 1969; Yao, 1974), recent studies tend to use the EF curve to determine θ_{crit} (e.g., Feldman et al., 2019; Fu et al., 2024), as EF is easier to estimate. An appropriate calculation of PET requires a series of assumptions (Koster et al., 2009). Therefore, alternative formulations such as grass reference ET (ET_0) and FAO-56 (The Food and Agricultural Organization (FAO) of the United Nations) based PET (PET_{FAO}) have been proposed (Allen et al., 1998). Accordingly, the ratio of ET_a to ET_0 (rET_0) and the ratio of ET_a to PET_{FAO} ($rPET_{FAO}$) can serve as alternatives to rPET (Peng et al., 2019; Qiu et al., 2020). The diversity in literature using EF, rET_0 or $rPET_{FAO}$ motivated us to analyze the impact of the chosen fitting relationship (i.e., EF-SM, rET_0-SM and $rPET_{FAO}$-SM) on estimated θ_{crit}. Additionally, linear-plus-plateau fitting curvesss likely simplify the relationship between SM and ET_a. In reality, this relationship might have a steep slope at the dry end and a more gentle slope at the wet end (Koster et al., 2024). Such consideration led us to extend the existing analyses of θ_{crit} by other functions. We aimed to investigate the sensitivity of θ_{crit} to these various fitting curves.

θ_{crit} mainly depends on soil properties and is impacted by vegetation and climate (Wankmüller et al., 2024). As the TERENO lysimeter networks span from the Northeast German lowlands to the Bavarian Alps, it enables the investigation of θ_{crit} across various soil textures, vegetation types and climatic conditions. More importantly, TERENO has implemented an observational approach based on a modified "space-for-time" concept to capture the impacts of changing climatic conditions on the soil–plant system (Pütz et al., 2016; Groh et al., 2022). The intact soil monoliths were transferred between stations and thus exposed to different climatic regimes, which means that soils are transferred in space rather than waiting at the same location for changes in climate over time (Groh et al., 2020a). Such a crossed soil type and climate experimental setup allows for isolating the climate alone and investigating the influence of changing climatic conditions on θ_{crit}. In our study, we specifically analyzed the impact of a change in aridity index (AI) defined as the ratio of mean annual ET_0 and precipitation.

Furthermore, according to FAO-56 guidelines, θ_{crit} (θ_{crit_FAO56}) is approximated as the midpoint between field capacity (FC) and wilting point (WP), which represents the readily available water that a crop can extract from the root zone without suffering from water stress (Allen et al., 1998). As FAO-56 estimates are often used in practice, for example for irrigation scheduling, it is important to evaluate the validity of this approach using θ_{crit} values derived from lysimeter measurements.

In summary, in this study, we explore, to our knowledge for the first time, the possibility of quantifying θ_{crit} using lysimeter measurements, which enables us to examine θ_{crit} by considering root zone SM rather than only near surface SM. This is the major novelty of this work. Additionally, we evaluate the robustness of θ_{crit} by applying different curve-fitting methods and examining the impact of climatic conditions. We seek to provide a thorough and detailed analysis of lysimeter-specific θ_{crit}, with the aim of answering the following main questions: (1) Does using the rET_0 definition and $rPET_{FAO}$ definition result in comparable θ_{crit} as using the EF definition? (2) Does θ_{crit} vary when using different fitting functions? (3) How does θ_{crit} derived from surface SM differ from θ_{crit} derived from root zone SM? (4) Does θ_{crit} change for the same ecosystem under different climatic conditions?

2. Materials and methods

In situ observations at lysimeter sites were used to determine the critical soil moisture thresholds (θ_{crit}), which marks the transition between the two distinguished regimes (a water-limited regime and an energy-limited regime). The analysis was performed on daytime observations over the growing seasons for each lysimeter. Daytime was defined as 9 a.m. to 5 p.m. at each site, based on the median diurnal cycle of net radiation. The growing season was defined as April to September for grass and mid-season stages for crops.

The flow chart of this study is shown in Fig. 2. In this section, the framework we first introduced (section 2.1) including the detection of soil drydowns during which the transition is most likely to happen, and the estimation of θ_{crit}. Section 2.2 gives an overview of lysimeter sites, followed by a description of the datasets used (section 2.3). Next, section 2.4 and section 2.5 present the computation of EF, rET_0 and $rPET_{FAO}$, respectively. The alternative fitting function is described in section 2.6. Finally, section 2.7 introduces root zone θ_{crit} according FAO-56.

2.1. A framework for estimating critical soil moisture thresholds

2.1.1. Drydown identification

The transition between energy-limited and water-limited regimes is most likely to occur during soil drydowns, i.e., periods when SM tends to show continuous incremental decrease in the absence of precipitation. Similar to McColl et al. (2017) and Akbar et al. (2018), the drydown selection process was automated on a daytime basis according to the following logic:

1) The drydown must begin after a precipitation event stops. This means that precipitation should be zero on the first day of the drydown period.
2) During a drydown event, precipitation should not exceed 1 mm/day.
3) During a drydown event, the soil moisture (SM) increments should be negative. However, noise can exist in observations. To avoid truncating a real drydown due to a single positive SM increment in a series of negative increments, positive SM increments less than 1% of the range of observed SM are excluded from the drydown event in order not to generate multiple drydown events. For example, in Fig. 3 the blue dots in the orange shadows refer to the SM which have positive increments and were excluded from the real drydown event.
4) The drydown must last for at least 5 days. This minimum length was chosen as a compromise between ensuring a large sample size and focusing on drydown events of relevant impact. The results did not reveal a strong difference when compared with a 9-day period suggested in previous studies (Akbar et al., 2018; Fu et al., 2024; McColl et al., 2017; Shellito et al., 2018).

The drydown selection process was performed separately for surface SM (θ_s) and root zone SM (θ_v). An illustrative example of SM time series is shown in Fig. 3 to highlight the drydowns identified by the above procedure based on observations from one lysimeter.

2.1.2. Estimation of critical soil moisture thresholds

Fig. 1 presents the framework of estimating θ_{crit}. The f_{ET}-SM relationship was built by using all the data pairs during drydowns over the growing seasons for each lysimeter and then fitted by a linear-plus-plateau model:

$$f_{ET} = \begin{cases} f_{max} + S(SM - \theta_{crit}) & if\ SM < \theta_{crit} \\ f_{max} & if\ SM \geq \theta_{crit} \end{cases} \quad (1)$$

where f_{ET} represents either EF, rET_0 or $rPET_{FAO}$. SM can be either θ_s or θ_v. θ_{crit} is the critical SM thresholds. f_{max} is the maximum value of f_{ET} in the energy-limited stage where SM is abundant and no longer the limiting factor for ET. In the "water world", ideally, the highest ceiling of rPET must be 1, which indicates that the plants don't suffer from water stress. However, such limitation was not imposed on the maximum value of rET_0 and $rPET_{FAO,}$ since ET_0 and PET_{FAO} are not necessarily the exact value of PET. S denotes the slope of the linear increase phase,

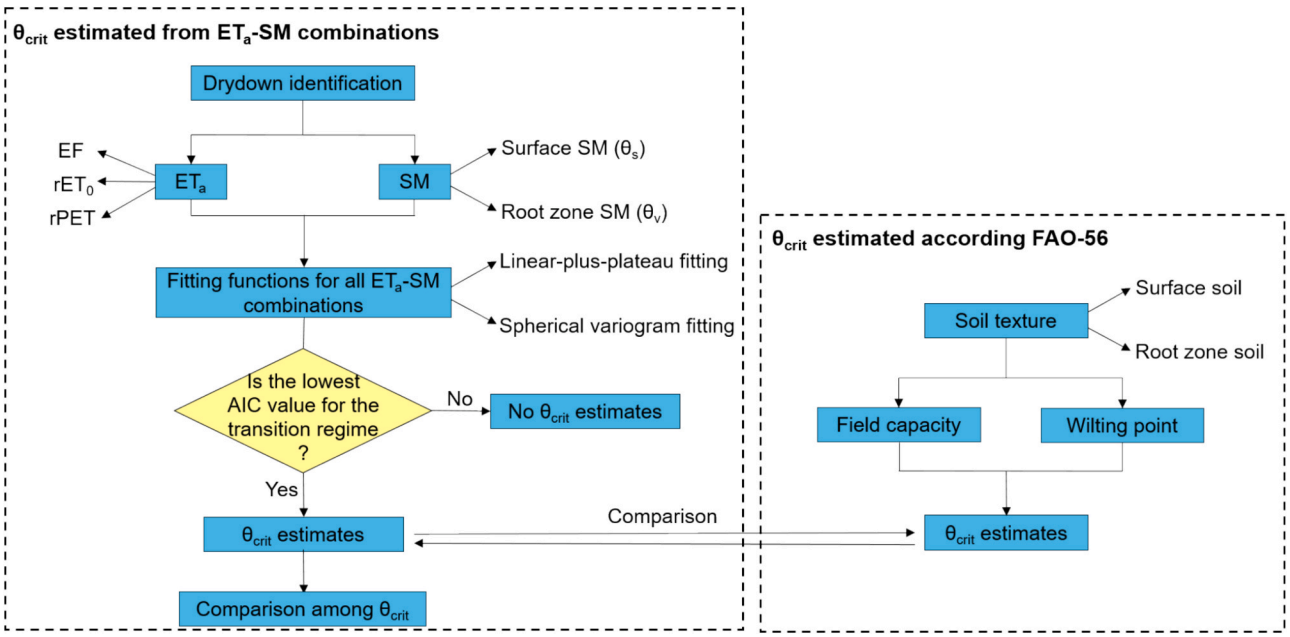

Fig. 2. Flow chart showing the estimation of critical soil moisture (θ_{crit}).

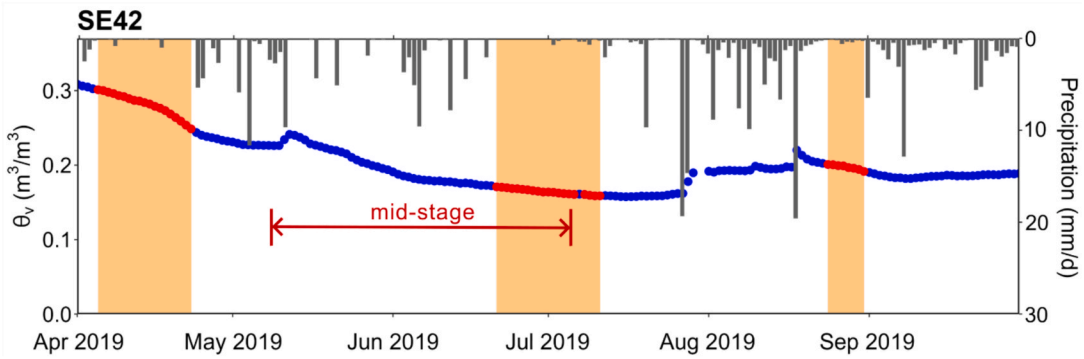

Fig. 3. Example time series of vertically integrated (0–60 cm) SM (θ_v) for one lysimeter (SE42) of the SEsb lysimeter group at the SE site for April-September 2019. Drydowns are highlighted in orange. θ_v during the drydown events are marked as red. Blue dots represent θ_v which are outside or excluded from the drydown events. Bars represent the daily precipitation.

indicating the sensitivity of f_{ET} to SM and thus the impact of SM on atmospheric conditions in the water-limited regime (Schwingshackl et al., 2017; Fu et al., 2022). θ_{crit} was estimated by a global optimization that minimizes the sum of squared errors, leading to lysimeter-specific estimated values. The optimization was performed with the "minpack.lm" package in the R programming language (Elzhov et al., 2015).

Previous studies considered two other linear models, one assuming that ET_a is purely water-limited, and one assuming a purely energy-limited regime (Feldman et al., 2019; Fu et al., 2024; Hsu and Dirmeyer, 2023a). Since all sites are located in Germany where water-limited conditions are rare, the purely water-limited model is not good as a null hypothesis. Therefore, the linear-plus-plateau model was only compared with the linear model for the purely energy-limited regime. The Akaike's Information Criteria (AIC) metric (Akaike, 1974) was used to determine the optimal model with the lowest AIC value. θ_{crit} is identified only when the linear-plus-plateau model is selected.

2.2. Site description and lysimeter set-up

A total of 61 lysimeters from seven sites of the TERENO-SOILCan network in Germany (Fig. 4, Table 1) were selected for this study. The distances between lysimeters vary from 0 to 680 km. The aridity index (AI) varied on average between these sites from 0.46 to 2.19, reflecting a range of climatic conditions from humid, sub-humid to semi-arid (Table 1). The soil texture of the surface soil and root zone soil varied and included clay, clay loam, sandy clay loam, sandy loam, silt loam and loam (Table 1). The dominant land cover for the lysimeters consists of grassland (natural and managed) and arable land (crop rotation). The grassland lysimeters are mainly composed of grasses, herbs or forest meadow. Detailed information on crop types, including planting and harvest dates for the arable land, is provided in Tables S2–S5 in Supplementary material 2.

At each site, there is at least one standardized hexagonal array of six individual cylindrical weighable lysimeters (UMS GmbH, Munich, Germany), each with a surface area of 1.0 m^2 and a depth of 1.5 m. The high-precision (resolution of 10 g, corresponding to a water depth ~0.01 mm) and high-resolution (1-minute measurements) lysimeters at the same site are situated only a few meters apart (approximately 3–6 m). Further technical specifications of the lysimeter used in this study are given in Pütz et al. (2016).

Based on the "space-for-time" concept, some local excavated lysimeters were transferred from their original sites to different climate regimes within and across TERENO observatories (Pütz et al., 2016). The spatial transfer of the intact soil monoliths in these lysimeters was

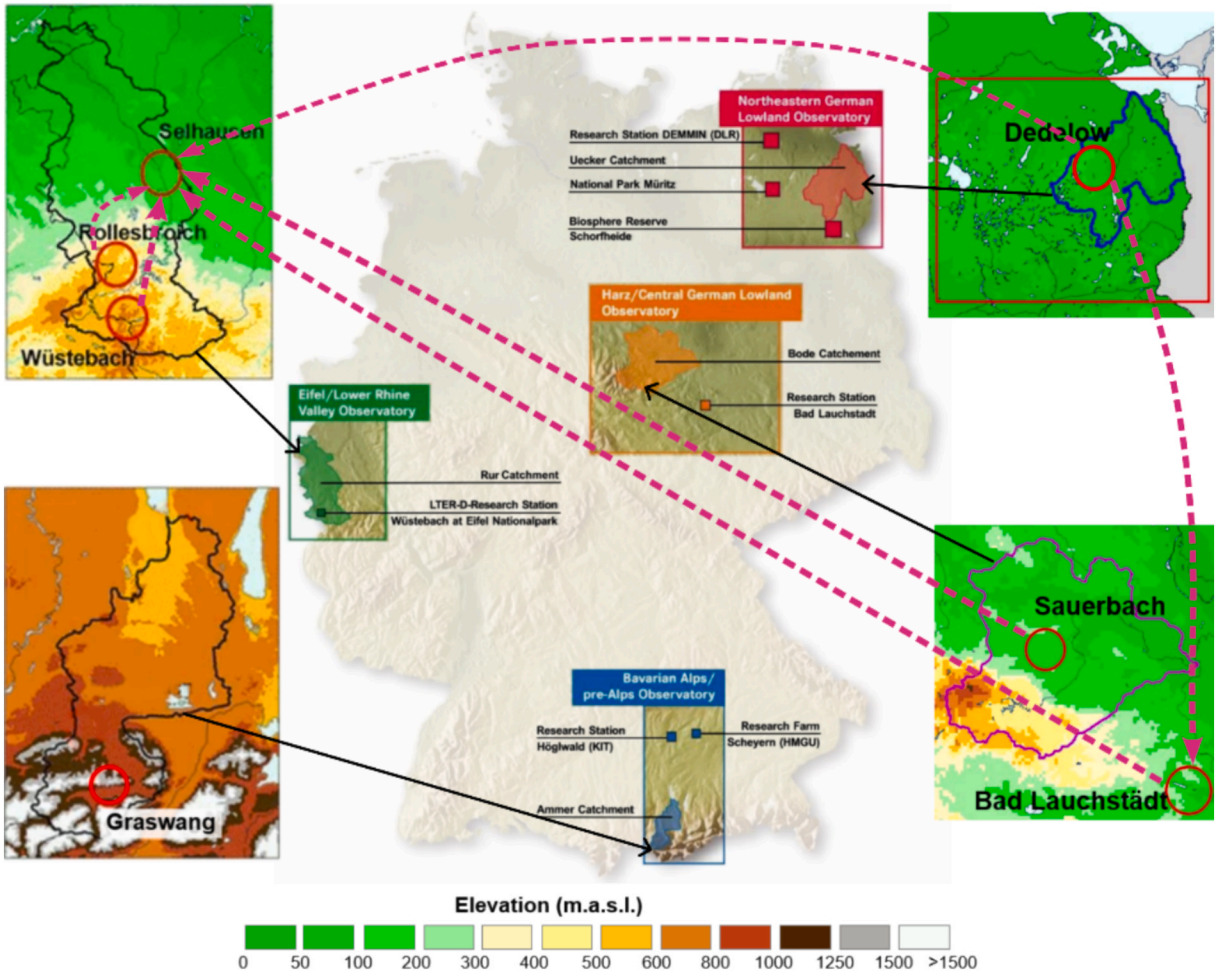

Fig. 4. Locations of the four TERENO observatories in Germany. The red circles marked in each observatory indicate the location of the lysimeter stations used in this study (adapted from Pütz et al. 2016). The pink dashed arrow line indicated the transfer routes of the soil monoliths.

intended to mimic changes in climatic conditions, characterized by an increased AI. This change in climatic conditions was abrupt due to the transfer of the soil monoliths in space, which differs from the standard "space-for-time" substitution approach in ecological or hydrological studies (e.g., Blois et al., 2013; Troch et al., 2015), that suggests gradual ecosystem changes over time. Instead, θ_{crit} for the same soil under different climatic conditions were compared. In this study, the lysimeters from the sites Rollesbroich (RO), Wüstebach (WU), Sauerbach (SB) and Graswang (GW) always contain the local soil, whereas for the sites Selhausen (SE), Dedelow (DD) and Bad Lauchstädt (BL), one lysimeter group contains the local soil, and other groups contain the soil from other sites (Table 1, Fig. 4). It should be noted that the soil monoliths transferred to the site DD (i.e., DDhd, DDck, DDcs, DDgk, DDgs, DDhk, DDhs, see Table 1) investigate the impact of past erosion processes on the soil ecosystem (Groh et al., 2020b), rather than the change in climatic conditions.

The climatic conditions at the transferred site and the original site are different in terms of AI including mean annual air temperature, ET_0 and precipitation. The original sites represent a long-term climate scenario to which the soil was exposed prior to translocation, whereas after the translocation, the soil was subject to the specific meteorological conditions of the transferred sites. Therefore, Table 2 summarizes the differences between the long-term climatological averages at the original site and the mean climate conditions observed during the study period at the transferred site. The AI differences ranged from 0.17 to 1.05. Additionally, the absolute differences ranged from 186 to 426 mm y^{-1} for annual ET0, 96–591 mm y^{-1} for mean annual precipitation and 1.8–4.4 °C for mean annual air temperature.

2.3. Data

2.3.1. Lysimeter ET_a

Lysimeter raw data were recorded at 1-minute intervals. Firstly, the raw lysimeter data underwent a manual and automatic plausibility check (Schneider et al., 2021). Secondly, the adaptive window and threshold filter was applied (AWAT; Peters et al., 2014, 2017) to reduce the impact of noisy lysimeter mass changes on the determination of precipitation and ET_a. In the next step, the ET_a data of the lysimeters were aggregated to hourly values. In this study, missing hourly ET_a values were partly gap-filled using linear regression with parallel ET_a values from other available lysimeters (same site and same soil). If parallel ET_a values are missing at that point in time, then ET_a at that point in time is not available and missing. Only days where ET_a was available for all daytime hours were considered in the analysis.

2.3.2. Soil moisture

SM was measured by the sensors (CS610 connected to a TDR100, both Campbell Scientific, North Logan, UT, USA) inside the lysimeters at 10-, 30- and 50-cm depths with a temporal resolution of 30 min (Groh et al., 2019). SM was averaged to daytime values (9 a.m. to 5 p.m.). Observations at 10 cm depth were regarded as θ_s. The 0–60 cm vertically integrated SM was considered as θ_v as most of the roots of the lysimeter plants are expected in the top 60 cm of the soil column. The SM measurements at 10, 30 and 50 cm depth were assumed to represent the soil

Table 1
Specifications of the lysimeters used in this study. For the lysimeter group, the first two letters represent the location of the lysimeters and the last two letters represent the soil origin. For the lysimeter ID, the first two letters indicate the site where the lysimeter is located, the first number indicates the lysimeter hexagon and the second number indicates the lysimeter of the hexagon. Sand fraction for soil depth 0–60 cm was weighted according the soil sample depths. Aridity index was calculated by mean annual grass reference ET divided by mean annual precipitation. There are four classifications according the aridity index: humid (Aridity index $\leq$ 1.3), sub-humid (1.3 < Aridity index $\leq$ 1.5), semi-arid (1.5 < Aridity index $\leq$ 5), and arid (5 < Aridity index < 20).

Site	Soil origin	Lysimeter group	Lysimeter number	Lysimeter ID	Latitude/ Longitude	Elev. (a.s. L.m)	Land cover type	Aridity index	Soil depth 0–10 cm		Soil depth 0–60 cm	
									Sand (%)	Texture class (USDA)	Sand (%)	Texture class (USDA)
Wüstebach (WU)	WU	WUwu	6	WU11-WU16	50.50N/ 6.33E	625	Grassland	0.46	39	Clay loam	46	Loam
Graswang (GW)	GW	GWgw	1	GW13	47.57N/ 11.03E	864	Grassland	0.62	9	Clay	8	Clay
Rollesbroich (RO)	RO	ROro	6	RO11-RO16	50.62N/ 6.30E	515	Grassland	0.78	52	Sandy clay loam	48	Sandy clay loam
Selhausen (SE)	French Technosol	SEfr	3	SE11,15,16	50.87N/ 6.45E	104	Grassland	1.43	71	Sandy loam	71	Sandy loam
	Scheyern	SEsy	3	SE12,13,14			Grassland		59 ± 3	Sany loam	58 ± 4	Sandy loam
	RO	SEro	3	SE21,25,26			Grassland		52	Sandy clay loam	48	Sandy clay loam
	WU	SEwu	3	SE22,23,24			Grassland		39	Clay loam	46	Loam
	BL	SEbl	3	SE31,35,36			Arable land		5	Silt loam	4	Silt loam
	SE	SEse	3	SE32,33,34			Arable land		13	Silt loam	11	Silt loam
	DD	SEdd	3	SE41,45,46			Arable land		56 ± 5	Sandy loam	54 ± 3	Sandy loam
	SB	SEsb	3	SE42,43,44			Arable land		13	Silt Loam	15	Silt loam
Dedelow (DD)	DD	DDdd	3	DD11,13,15	53.37N/ 13.80E	41	Arable land	1.7	49 ± 4	loam	50 ± 3	Loam
	Holzendorf	DDhd	3	DD12,14,16			Arable land		57 ± 6	Sandy loam	59	Sandy loam
	Christianenhof (exposed hilltops)	DDck	1	DD21			Arable land		55	Sandy loam	56	Sandy loam
	Christianenhof (topographic depressions)	DDcs	1	DD22			Arable land		65	Sandy loam	63	Sandy loam
	Grünow (exposed hilltops)	DDgk	1	DD23			Arable land		55	Sandy loam	54	Sandy loam
	Grünow (topographic depressions)	DDgs	1	DD24			Arable land		62	Sandy loam	58	Sandy loam
	Holzendorf (exposed hilltops)	DDhk	1	DD25			Arable land		61	Sandy loam	59	Sandy loam
	Holzendorf (topographic depressions)	DDhs	1	DD26			Arable land		70	Sandy loam	63	Sandy loam
Sauerbach (SB)	SB	SBsb	6	SB11-SB16	52.08N/ 11.28E	143	Arable land	2.07	13	Silt loam	15	Silt loam
Bad-Lauchstädt (BL)	DD	BLdd	3	BL21,23,25	51.39N/ 11.88E	118	Arable land	2.19	54 ± 3	Sandy loam	52 ± 2	Loam
	BL	BLbl	3	BL22,24,26			Arable land		5	Silt loam	4	Silt loam

column between 0–20, 20–40 and 40–60 cm depth respectively and were equally weighted to determine θ_v.

2.3.3. Meteorological data

Meteorological data including air temperature, air humidity, wind speed, air pressure and global radiation were obtained at each site from the lysimeter weather station (WXT510, Vaisala Oyj, Helsinki, Finland) for 10-min time steps. Precipitation was measured at RO, WU, and SE by a weighable gauge (Pluvio^2, Ott Hydromet, Kempten, Germany), and at GW, DD, SB and BL by a tipping bucket gauge (GW: WXT520, Vaisala; DD and SB: ecoTech Umwelt-Meßsysteme GmbH, Bonn, Germany; and BL: LAMBRECHT meteo, Göttingen, Germany). Precipitation was summed to daily values and other variables were averaged to hourly data prior to further computation. For those sites which have nearby stations whose data are available from the TERENO-portal (https://teodoor.icg.kfa-juelich.de/ibg3searchportal2/index.jsp), the time-series were gap-filled using the data from the online database with a stepwise gap-filling procedure (Giraud et al., 2021). Firstly, a linear regression was conducted with each station for each variable. Subsequently, the regression with the lowest root mean square error (RMSE) was used to fill the gaps until all the stations were used. As a result, gaps in the hourly meteorological data were filled for all sites, except the BL site, which only had a few gaps for two days.

A net radiation sensor (LP Net07, Delta OHM S.r.L., Caselle di Sevazzano, Italy) was installed above one lysimeter in each lysimeter group at each lysimeter site. Net radiation (Rn) was measured at a 10 min temporal resolution and aggregated to hourly data. The missing hourly Rn were gap-filled using the similar stepwise linear regression procedure as described above, but using Rn measurements from different lysimeter groups at the same site or from the corresponding eddy covariance (EC)

Table 2
Differences in mean annual grass reference ET (ET_0), mean annual precipitation (P), mean annual air temperature (Ta) and aridity index (AI, defined as the ratio of ET_0 to P) between the translocated and original sites. Site abbreviations: BL – Bad Lauchstädt; DD – Dedelow; RO – Rollesbroich; SB – Sauerbach; SE – Selhausen; WU – Wüstebach.

Translocated site	Original site	ΔAI	ΔET_0 (mm y^{-1})	ΔP (mm y^{-1})	ΔTa (°C)
SE	DD[#]	0.17	227	96	2.5
SE	BL[#]	0.18	253	115	1.8
SE	SB[#]	0.19	240	98	1.9
SE	RO[*]	0.81	254	−388	3.7
BL	DD[#]	0.93	186	−137	2.0
SE	WU[*]	1.05	426	−591	4.4

[#] Long-term means at the original sites (DD, BL and SB) were reported by Groh et al. (2016) for the period 1981–2010.

[*] For the RO and WU sites, long-term means were calculated over 1991–2010. Firstly, annual ET_0 was obtained from the grid maps from the German Weather Service (DWD, https://www.dwd.de), while annual P and Ta were derived from a nearby weather station (Kall-Sistig) from DWD. Secondly, the annual ET_0, P and Ta were adjusted using linear regression with in-situ observations at the study sites based on overlapping years to correct for site-specific values. Finally, the mean annual values for the period 1991–2010 are as follows: at the RO site, ET_0 was 633 mm y^{-1}, P 1006 mm y^{-1}, and Ta 7.70 °C; at the WU site, ET_0 was 460 mm y^{-1}, P 1209 mm y^{-1}, and Ta 7.04 °C.

station nearby.

2.3.4. Surface soil heat flux

Directly measuring surface soil heat flux (G_0) is challenging because soil heat flux plates have to be buried at a subsurface depth in the soil to avoid potential effects of soil-atmosphere processes (Gao et al., 2017). In this study, one soil heat flux plate (HFP-01, Hukseflux Thermal Sensors B.V., Delft, the Netherlands) was installed at 10 cm depth inside each lysimeter to measure the soil heat flux (G_{10}). The calorimetric method was applied to calculate G_0 according to the following equations (Ding et al., 2010; Giambelluca et al., 2009; Li et al., 2022):

$$G_0 = G_z + \Delta S \tag{2}$$

$$\Delta S = \frac{T_{s,i} - T_{s,i-1}}{t} z(C_{vs} + C_{vw}\theta) \tag{3}$$

where G_z is the soil heat flux measured at a depth of z m (W m^{-2}; here G_z is G_{10} with z equal to 0.1 m), ΔS is the heat storage between the soil surface and the heat flux plate (W m^{-2}), t is the time interval (3600 s), C_{vw} is the volumetric heat capacity of water (4190 KJ m^{-3} K^{-1}), and C_{vs} is the volumetric heat capacity for the soil solid portion with a value of 1420 KJ m^{-3} K^{-1}.$T_{s,i} - T_{s,i-1}$ (K) is the soil temperature (T_s) difference between time steps i and i-1 for the soil layer above the soil heat flux plate, θ is the volumetric soil moisture content in the soil layer above the soil heat flux plate (m^3 m^{-3}).

Note that there are no sensors measuring T_s and θ in the layers between soil surface and soil heat flux plates in the lysimeters — the shallowest only at the same depth (10 cm) as the flux plates. Therefore, T_s and θ at 10 cm were utilized for the calculation for each lysimeter, except for the lysimeters at the SE site, where T_s sensors were not functioning during the study period. Thus, for the SE site, the average T_s measurements were used from three sensors at 5 cm depth from the lysimeter field which is covered by grass. Prior to the computation of G_0, G_{10}, T_s and θ were gap-filled with parallel measurements (same soil and same site) following the stepwise gap-filling procedure.

It is acknowledged that the determination of G_0 may not be highly accurate. However, a sensitivity analysis on G_0 estimation was conducted using different input data sets and parameters and the calculated G and the measured G at 3 cm depth (G_{03}) at the RO site were compared (Supplementary Material 1). The results show that the different approaches have a similar performance and small differences between calculated G_{03} and measured G_{03}, providing confidence in the above calculation. In addition, since G_0 is a relatively small flux compared to LE and Rn during daytime, possible bias in G_0 does not have a large impact on the EF results and therefore does not affect θ_{crit}.

2.4. Energy world (Evaporative fraction)

EF is a non-dimensional variable that characterizes the land surface partitioning of available energy for exchange with the overlying atmosphere. EF was calculated on the same daytime basis in this analysis:

$$EF = \frac{LE}{LE + H} \tag{4}$$

where LE and H are daytime mean latent and sensible heat fluxes (W m^{-2}). H was treated as the residual of the energy balance. It can be estimated as:

$$H = R_n - G_0 - LE \tag{5}$$

H was calculated on an hourly basis in Eq. (5) and then aggregated to daytime values before calculating EF in Eq. (4). If there are missing values for LE or H during daytime, the day is excluded from the analysis. As EF shows large uncertainty, the EF was also restricted to the range of 0–1 to remove outliers, as in previous studies (Schwingshackl et al., 2017; Dong et al., 2023).

2.5. Water world (Ratio of actual to potential ET)

2.5.1. Grass reference ET

The ET_0 calculation is needed for both the rET_0 and $rPET_{FAO}$ methods. Hourly ET_0 was calculated with the FAO Penman-Monteith equation (Allen et al., 2006):

$$ET_0 = \frac{0.408\Delta(R_n - G_0) + \gamma \frac{37}{T_h + 273} u_2 (e^o(T_h) - e_a)}{\Delta + \gamma(1 + C_d u_2)} \tag{6}$$

where Δ is the slope of the vapor pressure curve (kPa $°C^{-1}$), T_h is mean hourly air temperature at 2 m height (°C), $e^o(T_h)$ is hourly saturation vapor pressure (kPa), e_a is hourly actual vapor pressure (kPa), γ is psychrometric constant (kPa $°C^{-1}$), C_d is a coefficient with a value of 0.24 s m^{-1} when $R_n > 0$ and 0.96 s m^{-1} when $R_n < 0$, and u_2 is wind speed at 2 m height (m s^{-1}), and G_0 is estimated based on Eq. (2).

2.5.2. Determination of mid-season stage for crops

For crops, only the mid-season stages were considered in the analysis. This is because at mid-season stages, most of the soil surface on the lysimeters is covered by the crop (crop coefficient is maximum) and water loss is mainly due to crop transpiration. Therefore, it is important to know the length of mid-season stages for each crop season. FAO-56 provided tabulated crop growing lengths (initial stage, development stage, mid-season stage and late stage) for various crops in many parts of the world. Firstly, a similar crop listed in the FAO-56 was identified (Table S1 in Supplementary material 2). With the actual sowing and harvest dates recorded for the crops on each lysimeter, the total length of the crop season was determined. Then a factor, which is the ratio of the actual total length to the length specified in FAO-56, was applied to adjust the length of each plant development stage accordingly (Tables S2–S5 in Supplementary material 2). For example, winter wheat planted on 2018-11-5 at the arable land lysimeters at the SE site and harvested on 2019-7-24, had a total length of 261 days. According to FAO-56, winter wheat planted in October in Idaho, USA, has a total length of 335 days, with a mid-season stage of 75 days. Applying a factor of 0.78 (i.e. 261 divided by 335), the mid-season length for this winter wheat was determined to be 58 days, as indicated in Fig. 3.

Such a calculation was performed for each crop and each crop season at each lysimeter site. Detailed information is provided in Supplementary material 2.

2.5.3. Crop coefficients

According to FAO-56, PET_{FAO} during mid-season stage is estimated from a single crop coefficient (K_{c_mid}) and ET_0 as in Eq. (7):

$$PET_{FAO} = K_{c\_mid} ET_0 \quad (7)$$

Since localized K_{c_mid} values are not always available, the values of K_{c_mid} as suggested by FAO-56 are being widely used to estimated PET_{FAO}. Therefore K_{c_mid} values from FAO-56 for each lysimeter were applied (Table S1 in Supplementary material 2).

2.6. Spherical variogram fitting

As the experimental data show a smoother curve rather than straight lines, it is worth exploring another fitting curve beyond the linear-plus-plateau fitting. The spherical variogram model which is a widely used approach in geostatistics (Mälicke et al., 2018; van Groenigen, 2000) was selected and applied in this study to describe SM- f_{ET}. This model was chosen because its shape aligns with the relationship of SM- f_{ET} (EF, rET_0 or $rPET_{FAO}$), which exhibits a linear behavior at small SM near the origin but flattens out at larger SM values, eventually reaching a plateau, or sill. A spherical variogram curve is expressed as:

$$f_{ET} = \begin{cases} 0 & SM = 0 \\ C_0 + C\left(\frac{3}{2}\frac{SM}{a} - \frac{1}{2}\frac{(SM)^3}{a^3}\right) & 0 < SM \le a \\ C_0 + C & SM > a \end{cases} \quad (8)$$

where C_0 is the nugget constant, $C_0 + C$ is the plateau, which in this study is the maximum value of f_{ET}, and defines the range of SM in the water-limited regime. Similar to the linear-plus-plateau fitting, the parameters a, C_0 and C could be simultaneously estimated using "minpack.lm" package in R. Note that it is common practice to define an effective range where 95% of the end value is reached (Oliver et al., 2015; Wadoux et al., 2019). Therefore, θ_{crit} is not equal to a, but is defined at a point where f_{ET} reaches 95% of the plateau. Thus, the θ_{crit} can be derived from the following equation:

$$C_0 + b\left(\frac{3}{2}\frac{\theta_{crit}}{a} - \frac{1}{2}\frac{\theta_{crit}^3}{a^3}\right) = 0.95(C_0 + C) \quad (9)$$

This cubic equation (Eq. (9)) was solved using the "uniroot" function in software R.

The performance of the linear-plus-plateau fitting or spherical variogram fitting was evaluated using the coefficient of determination (R^2). The Wilcoxon test was applied to determine if the change of the θ_{crit} among curve-fitting methods or for different SM depths or between lysimeters is statistically significant. The root mean square deviation (RMSD) was used to assess the differences in θ_{crit} among different curve-fitting methods or SM depths.

$$RMSD = \sqrt{\frac{1}{n}\sum_{i=1}^{n}(y_i - x_i)^2} \quad (10)$$

where x_i and y_i are the θ_{crit} estimates from different curve-fitting methods or SM depths, and n is the total number of estimates.

2.7. Critical root zone soil moisture thresholds according FAO-56

FAO-56 provides a range of typical FC and WP values across various soil textures, allowing for the calculation of θ_{crit_FAO56} ranges for different soil textures. However, for sandy clay loam, no specific ranges for FC and WP were provided in FAO-56. Instead, Raes et al. (2023) reported fixed values of 0.32 m^3/m^3 for FC and 0.2 m^3/m^3 for WP. To derive a comparable range of θ_{crit_FAO56} for sandy clay loam, the same uncertainty was assumed in FC and WP as observed for silt clay loam. Table 3 presents the range of FC, WP and calculated θ_{crit_FAO56} for different soil textures.

Table 3
The lower and upper values for field capacity (FC) and wilting point (WP) according to FAO-56, and the range of root zone critical soil moisture thresholds (θ_{crit_FAO56}) calculated from the midpoint of FC and WP. Note: values for Sandy clay loam are based on values from Raes et al. (2023).

Soil texture	FC (m^3/m^3)		WP (m^3/m^3)		θ_{crit_FAO56} (m^3/m^3)	
	lower	upper	lower	upper	lower	upper
Sandy loam	0.18	0.28	0.06	0.16	0.120	0.220
Loam	0.2	0.3	0.07	0.17	0.135	0.235
Silt loam	0.22	0.36	0.09	0.21	0.155	0.285
Silt clay loam	0.3	0.37	0.17	0.24	0.235	0.305
Sandy clay loam	0.285	0.355	0.165	0.235	0.225	0.295

3. Results

3.1. Consistency of θ_{crit} derived from the EF, rET_0 and $rPET_{FAO}$ definitions

We estimated θ_{crit} using the EF, rET_0 and $rPET_{FAO}$ definitions fitted by the linear-plus-plateau curve based on soil drydowns observed during growing seasons for each lysimeter (Figs. S1-S10 in Supplementary Materials 2). Out of a total of 61 lysimeters, there were 38 lysimeters with θ_{crit} estimates for surface soil and 35 for root zone soil from the EF definition (Table 4). The rET_0 definition provided the most estimates, with θ_{crit} determined for surface soil at 47 lysimeters and for root zone soil at 49 lysimeters. The $rPET_{FAO}$ definition had the fewest estimates, providing θ_{crit} for 30 lysimeters for the surface soil and 33 for the root zone soil, respectively. This is because the $rPET_{FAO}$ definition was performed only on crop lysimeters. Overall, more than 50% of the lysimeters had θ_{crit} values.

Among the sites, only for the GW site no drydown event was detected, and thus no θ_{crit} could be determined for any of the three definitions (Table 4). This is primarily due to the very wet conditions at this alpine site, as well as the greatly reduced number of data pairs caused by lysimeter disturbance related to chamber measurements. The SE site, which has the most lysimeters with 6 different lysimeter groups, had the highest numbers of θ_{crit} estimates. Fig. 5(a–c) shows examples of one crop lysimeter (SE42, i.e. the second lysimeter of the fourth hexagon at the Selhausen site) for each ET definition and for both surface and root zone soil using linear-plus-plateau fitting.

For the surface soil, the mean θ_{crit} across all the lysimeters was 0.168 ± 0.058 m^3/m^3 for the EF definition, 0.170 ± 0.044 m^3/m^3 for the rET_0 definition, and 0.160 ± 0.042 m^3/m^3 for the $rPET_{FAO}$ definition (Fig. 6a). However, the latter was only applied to lysimeters on which arable crops were grown. The highest θ_{crit} value using the EF definition was detected in the grass lysimeter WU13 at the WU site, with a value of 0.364 m^3/m^3, while the lowest θ_{crit} value was for the crop lysimeter DD14 at the DD site (0.088 m^3/m^3). For the rET_0 definition, the grass lysimeter RO13 at the RO site had the highest value of θ_{crit} (0.280 m^3/m^3), whereas the grass lysimeter SE13 showed the lowest (0.094 m^3/m^3). The $rPET_{FAO}$ definition, applied only to crop lysimeters, yielded the highest θ_{crit} value of 0.255 m^3/m^3 for the lysimeter SE35 at the SE site, and the lowest value of 0.096 m^3/m^3 for the lysimeter DD26 at the DD site.

For the root zone soil, the mean θ_{crit} across all the lysimeters was 0.206 ± 0.068 m^3/m^3 for the EF definition, which was similar to the mean θ_{crit} for the rET_0 definition (0.207 ± 0.052 m^3/m^3, Fig. 6a). The mean θ_{crit} for the $rPET_{FAO}$ definition which was only applicable to arable crops was slightly lower, with a value of 0.188 ± 0.041 m^3/m^3. The EF definition estimated the highest θ_{crit} value in the grass lysimeter WU13 at the WU site (0.355 m^3/m^3), while the lowest θ_{crit} value was for the crop lysimeter DD24 at the DD site (0.124 m^3/m^3). Both the rET_0 definition and the $rPET_{FAO}$ definition identified the lowest θ_{crit} value of

Table 4
Number of θ_{crit} estimates for surface or/and root zone soil at each site by the EF, rET_0 and $rPET_{FAO}$ definitions fitted by linear-plus-plateau curve.

Site	Surface soil			Root zone soil			All		
	EF	rET_0	$rPET_{FAO}$	EF	rET_0	$rPET_{FAO}$	EF	rET_0	$rPET_{FAO}$
GW	0	0	0	0	0	0	0	0	0
WU	1	1	0	2	1	0	3	2	0
RO	6	5	0	4	5	0	10	10	0
SE	17	21	10	16	24	12	33	45	22
BL	3	6	6	3	5	6	6	11	12
SB	0	2	2	0	4	4	0	6	6
DD	11	12	12	10	10	11	21	22	23
Sum	38	47	30	35	49	33	73	96	63

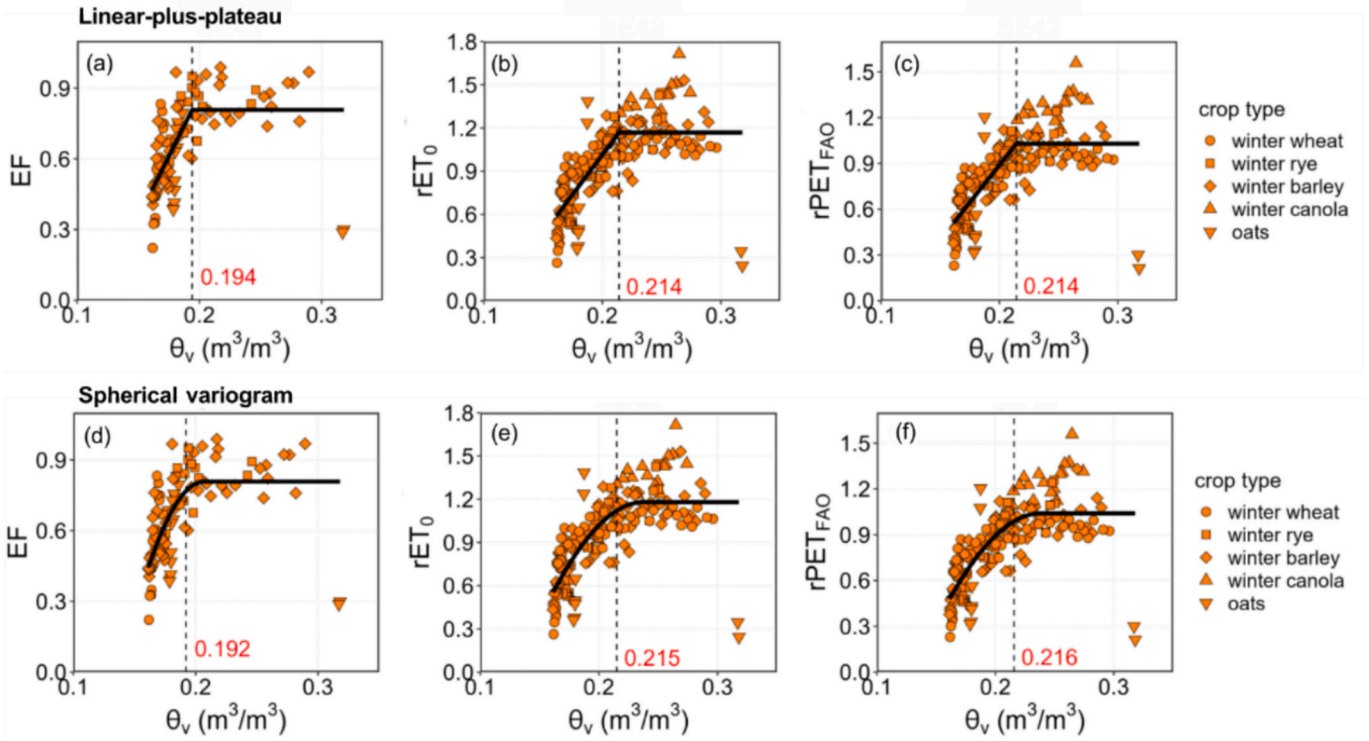

Fig. 5. Critical soil moisture thresholds (θ_{crit}) estimated from the root zone soil moisture (θ_v) for one crop lysimeter SE42 at the SE site filled with soil from the SB site using the EF, rET_0 and $rPET_{FAO}$ definitions by (a-c) linear-plus-plateau fitting and (d-f) spherical variogram fitting. In each plot, the shape of the dots indicates the crop type. The thick black line in each plot indicates the fitted curve. The red numbers in each plot indicate the estimated θ_{crit}.

0.127 $m^3/m^3$for the lysimeter DD22 at the DD site. For the rET_0 definition, the grass lysimeter RO13 at the RO site had the highest θ_{crit} (0.324 m^3/m^3), whereas for the $rPET_{FAO}$ definition, the highest value of θ_{crit} (0.302 m^3/m^3) was obtained from the crop lysimeter SB14 at the SB site.

Fig. 7 shows the comparison of lysimeter-specific θ_{crit} estimated using the three definitions (EF, rET_0, and $rPET_{FAO}$) both for surface soil and root zone soil. There was no significant difference in θ_{crit} across the three methods ($p > 0.05$), given a certain lysimeter and measurement depth (either surface SM or root zone SM). The RMSD between the rET_0 and EF definitions was 0.011 m^3/m^3 for crop lysimeters and 0.02 m^3/m^3 for grass lysimeters (Fig. 7a). The mean difference in θ_{crit} between the two definitions was 0.003 m^3/m^3 across all lysimeters, with 94% of the difference falling within the range of −0.01 and 0.01 m^3/m^3 (Fig. 7d). The θ_{crit} estimates of rET_0 and $rPET_{FAO}$ definitions were nearly identical for crop lysimeters, with 97% of the difference falling between −0.01 and 0.01 m^3/m^3 and 66% of the estimates being exactly the same (Fig. 7f). This is because for crops, PET_{FAO} is ET_0 multiplied by crop coefficients during mid-season stages, so the relationship between $rPET_{FAO}$ and SM is not expected to change significantly compared to that between rET_0 and SM. The RMSD for EF-$rPET_{FAO}$ relation is 0.011 m^3/m^3. Overall, most of the data points were closely distributed around the 1:1 line, with all three definitions showing consistent results (RMSD < 0.02 m^3/m^3, Fig. 7), indicating the reliability of the three definitions.

3.2. *Comparison between the linear-plus-plateau and spherical variogram fitting curves*

Fig. 5(d–f) shows the relationship between SM and EF, rET_0 or $rPET_{FAO}$ from the example crop lysimeter SE42 fitted by spherical variogram. Fig. 6b presents the θ_{crit} estimated from the spherical variogram fitting for each definition and each soil depth. Fig. 8 compares the lysimeter-specific results between linear-plus-plateau fitting and spherical variogram fitting. Though spherical variogram fitting provides a smoother fit in the water-limited regime (Fig. 5), there was no significant difference ($p > 0.05$) in the derived θ_{crit} values, plateau value or the performance of the fitting (R^2) compared to the linear-plus-plateau fitting (Fig. 8). The data points aligned closely with the 1:1 line, and 69% of the difference in θ_{crit} fell within the range of −0.01 to 0.01 m^3/m^3, suggesting that the θ_{crit} estimates are robust. This indicates that the

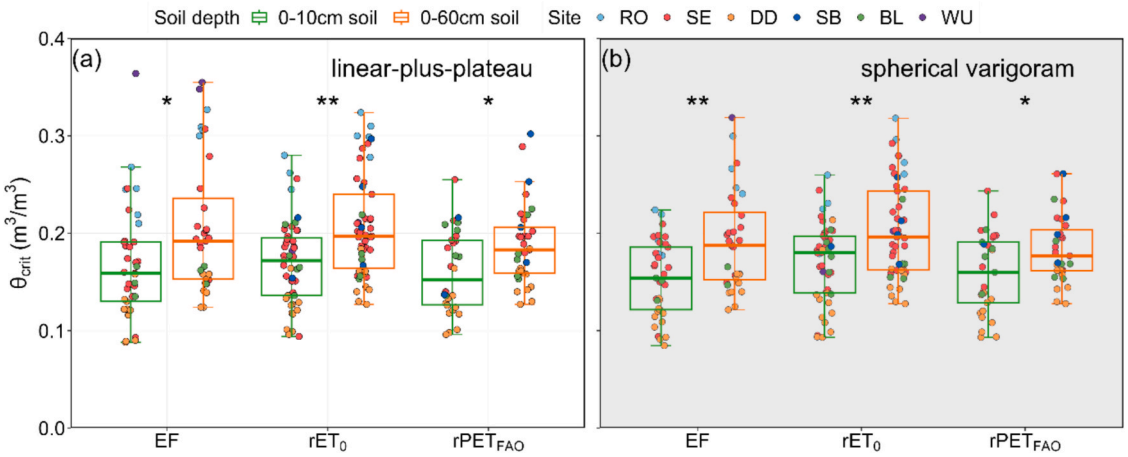

Fig. 6. θ_{crit} for surface soil (0–10 cm) and root zone soil (0–60 cm) according to the rET_0, EF and $rPET_{FAO}$ definition using (a) linear-plus-plateau fitting and (b) spherical variogram fitting. The middle line represents the median θ_{crit} estimated by a given definition based on values for individual lysimeters (indicated by dots); the box represents the upper and lower quartiles, and the whiskers represent 1.5 times the interquartile range. The color of the dots indicates the lysimeter sites. Black stars above the boxplots represent statistically significant differences of θ_{crit} between the surface soil and root zone soil using Wilcoxon test. * represents $p < 0.05$, ** represents $p < 0.01$, and *** represents $p < 0.001$. There was no significant difference in θ_{crit} estimates from different fitting curves or ET_a definitions ($p > 0.05$).

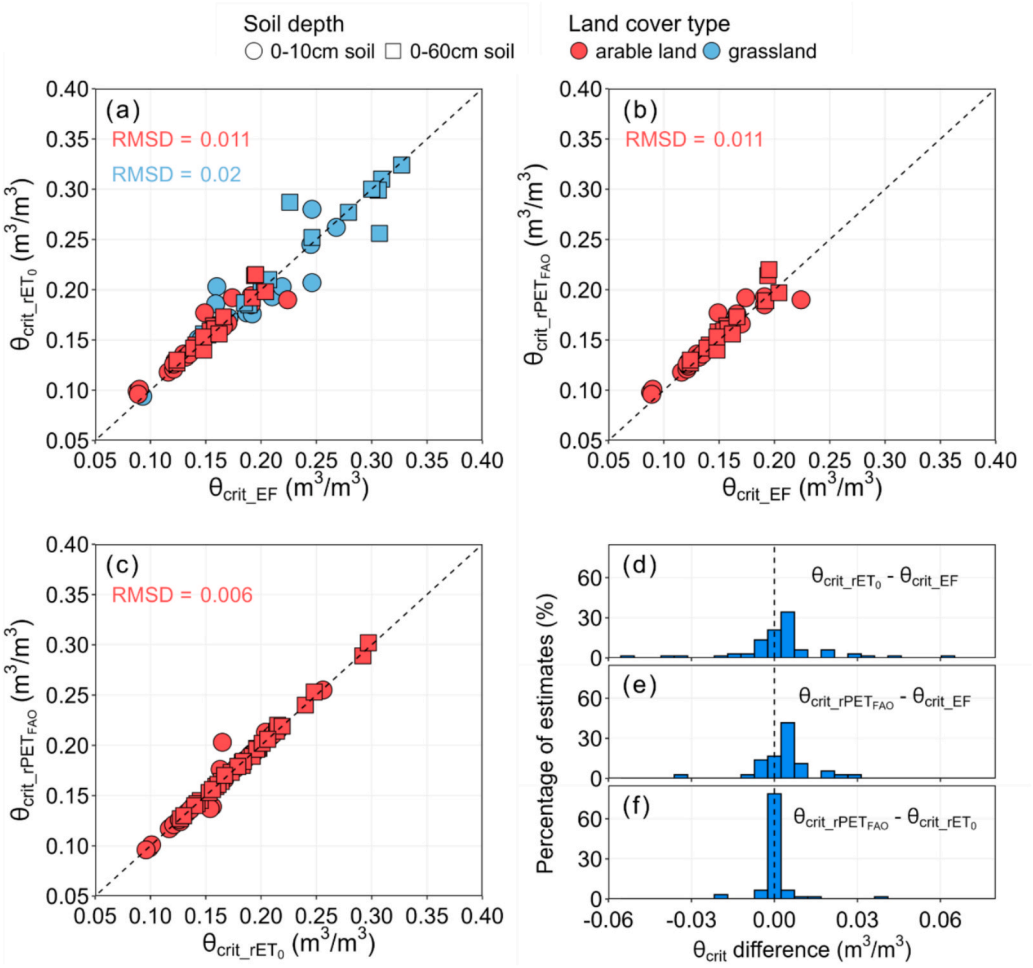

Fig. 7. (a–c) Comparison between lysimeter-specific θ_{crit} estimated according EF, rET_0 and $rPET_{FAO}$ definitions using linear-plus-plateau fitting. RMSD is the root mean square deviation of θ_{crit} estimates between the definitions. The dashed line is the 1:1 line. The shape of the dots represents the soil depth and the color of the dots indicates the land cover type. (d–f) Distribution of differences in θ_{crit} according the different definitions.

smoother nature of the spherical fitting does not impact the accuracy or consistency of the θ_{crit} estimates.

3.3. Comparison between surface and root zone θ_{crit}

Across all the lysimeters, the θ_{crit} for the root zone soil was

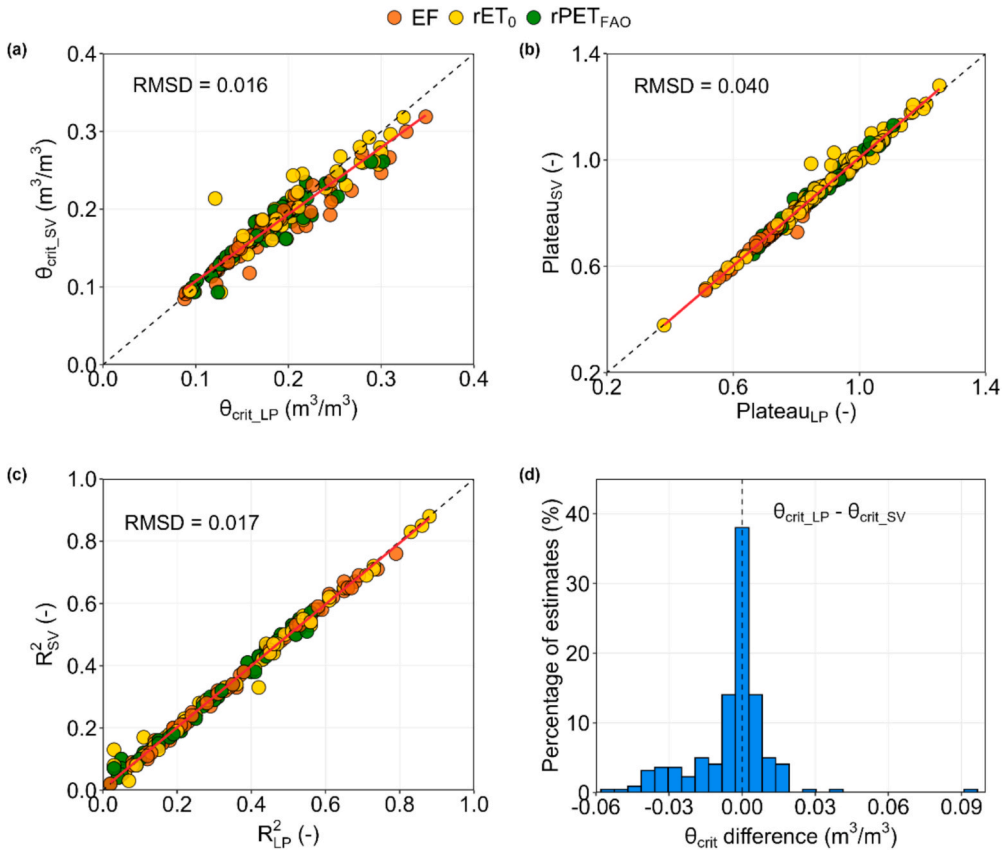

Fig. 8. Comparison between the linear-plus-plateau fitting and spherical variogram fitting regarding (a) θ_{crit}, (b) the plateau value of the fitting and (c) the performance of fitting based on values for individual lysimeters for each definition (EF, rET_0 and $rPET_{FAO}$) and soil depth (surface soil and root zone soil). The color indicates the definitions. Dashed line is 1:1 line and red line is the regression line. RMSD is the root mean square deviation. (d) Distribution of differences in θ_{crit} derived from the two fitting curves.

significantly higher than for the surface soil ($p < 0.05$), regardless of the three ET definitions or the two fitting curves (Fig. 6). Given the robust estimates by each definition and each fitting curve, in the following, we mainly focus on the θ_{crit} detected from the rET_0 definition using the linear-plus-plateau fitting as it provided the highest number of estimates.

Fig. 9 compares the lysimeter-specific θ_{crit} estimated using the rET_0 definition between the surface soil and root zone soil. Most of the data points were above the 1:1 line, with a RMSD of 0.046 m^3/m^3, indicating a higher θ_{crit} value for the root zone soil (Fig. 9a). As shown in Fig. 9b, the differences between root zone and surface θ_{crit} mostly ranged from 0 to 0.1 m^3/m^3. Despite these differences, the θ_{crit} for the surface soil and for the root zone soil showed a good correlation ($r = 0.83$, Fig. 9a).

Fig. 10 shows the relation between θ_{crit} and sand fraction for both surface and root zone soil. Overall, both surface and root zone θ_{crit} showed a declining trend with increasing sand fraction; however, the slope is significant only for surface θ_{crit} ($p < 0.05$). This can be explained by the fact that the hydraulic conductivity of coarser soils decreases at

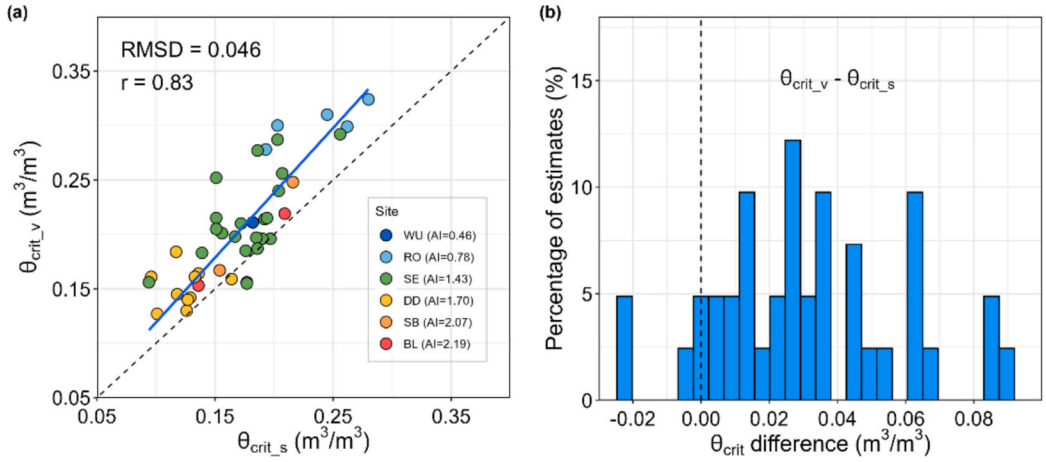

Fig. 9. (a) Scatterplot of θ_{crit} for surface soil (θ_{crit_s}) versus root zone soil (θ_{crit_v}), estimated for each lysimeter using the rET_0 definition. AI means aridity index. (b) Distribution of differences in θ_{crit} between root zone soil and surface soil.

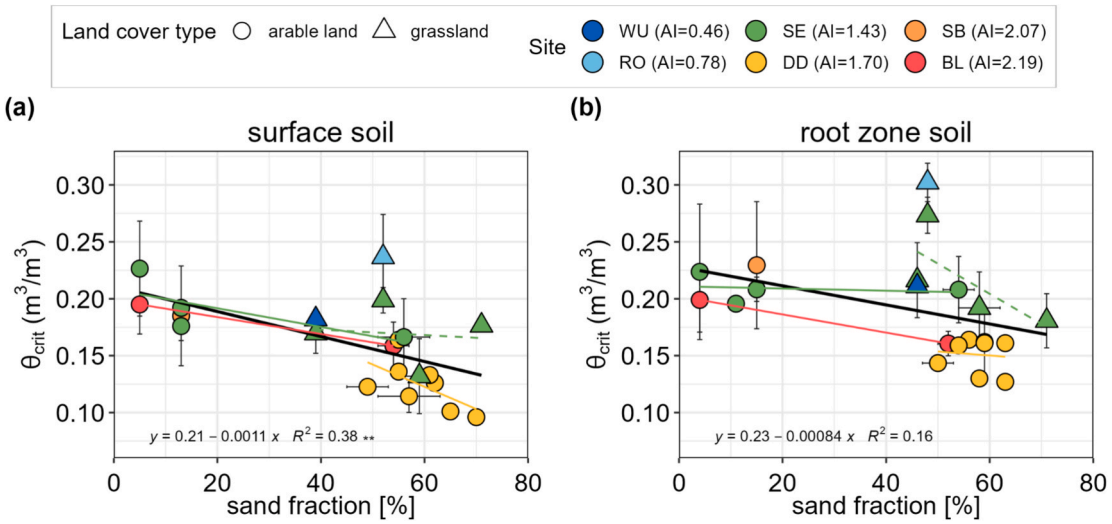

Fig. 10. Relationship between sand fraction and θ_{crit} for (a) surface soil and (b) root zone soil. The thick black line represents the linear regression of θ_{crit} to sand fraction for all lysimeter groups. Regression equations, R^2 and p-values (regression *t*-test) are indicated (**P < 0.01). Colored regression lines indicate the relationships between θ_{crit} and sand fraction for lysimeter groups that have the same land cover type at the same site but differ in soil texture.

lower water contents (but then decreases very quickly; Wankmüller et al., 2024). At the DD, BL and SE sites, there were lysimeters containing different soils but the same vegetation type, allowing the investigation of the impact of sand fraction on θ_{crit} without confounding effects from climate and ecosystem. Under identical climate, sand fraction had a smaller influence on root zone θ_{crit} compared to surface θ_{crit} for arable land given the gentler slope. Conversely, for grassland, the effect of sand fraction on root zone θ_{crit} was more pronounced than on surface θ_{crit}.

Across the sites, some lysimeters were translocated to emulate the expected changes in climatic conditions following the "space-for-time" concept. Fig. 11 shows the relation between θ_{crit} and aridity index. When the lysimeters were transferred to a drier site (with higher aridity index), the θ_{crit} both for the surface soil and root zone soil generally decreased (though not statistically significantly), except for the lysimeters with the DD soil at the SE site compared to the DD site. The reduction in θ_{crit} at drier sites could be attributed to plant self-regulation, such as adaptation of the root system or altering plant community composition to increase drought tolerance. For example, when lysimeters were moved from the humid RO site (ROro) to the sub-humid SE site (SEro), the mean surface soil θ_{crit} for the surface soil decreased from 0.245 to 0.203 m^3/m^3. In a study comparing the ROro and SEro lysimeters (Jarvis et al., 2022), it was found that the root depth was increased from ca. 56 cm at the RO site to ca. 80 cm at the SE site, and significant changes were observed in the plant community composition.

3.4. *Comparison of root zone θ_{crit} derived from observations and FAO-56*

The lysimeters with estimated θ_{crit} contained four different soil textures, namely sandy loam, loam, silt loam and sandy clay loam. Fig. 12 shows the comparison of root zone θ_{crit} estimated from lysimeter observations and calculated from FAO-56 for these soil textures. Sandy loam has the lowest median θ_{crit} of 0.164 m^3/m^3, whereas sandy clay loam has the highest median θ_{crit} of 0.291 m^3/m^3. Generally, the lysimeter-specific θ_{crit} values fall within the range of θ_{crit} estimated from FAO-56, which uses the midpoint between field capacity and wilting point. However, for sandy clay loam, which is the soil from the RO site,

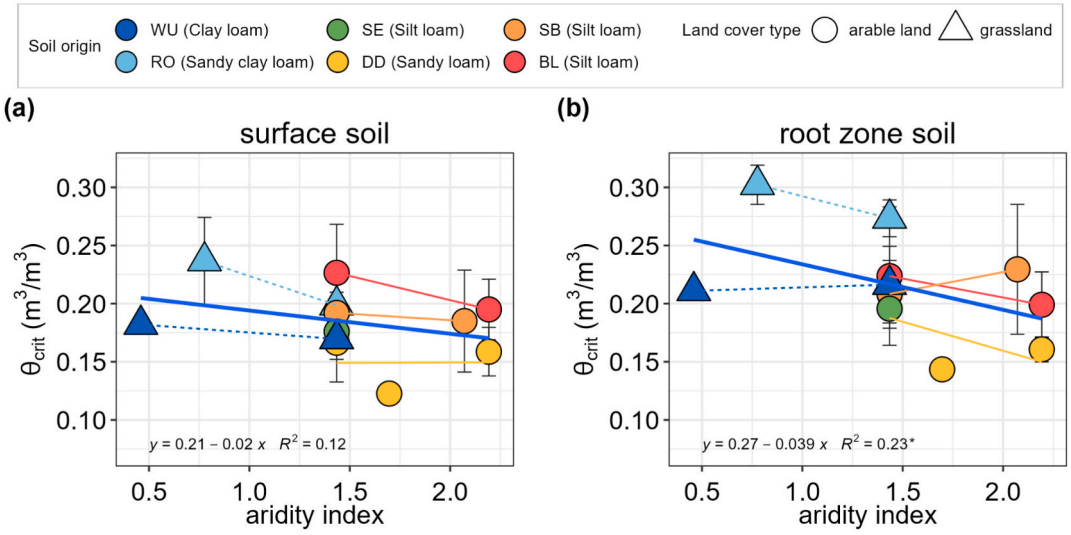

Fig. 11. Relationship between aridity index and θ_{crit} for (a) surface soil and (b) root zone soil. The thick blue line represents the linear regression of θ_{crit} to aridity index for all the translocated lysimeter groups. Regression equations, R^2 and p-values (regression *t*-test) are indicated (*P < 0.05). Colored regression lines indicate the relationships between θ_{crit} and aridity index for translocated lysimeters which have the same soil origin but are placed at different sites.

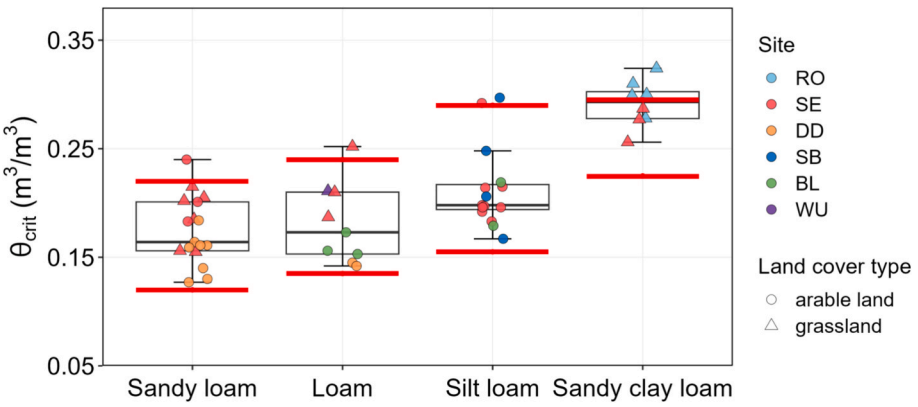

Fig. 12. Root zone θ_{crit} for different soil textures. The middle line represents the median θ_{crit} estimated for a given soil texture on the basis of values for individual lysimeters for that soil texture; the box represents the upper and lower quartiles and the whiskers represent 1.5 times the interquartile range. The shape of the dots indicates the land cover type of the lysimeters. Red lines indicate the upper and lower θ_{crit} calculated based on FAO-56.

the θ_{crit} values for some lysimeters are outside (above) the FAO-56 range. Notably, θ_{crit} for the lysimeters at the SE site (SEro lysimeters) are within the FAO-56 range, whereas θ_{crit} for the lysimeters at the RO site (ROro lysimeters) are generally above the upper limit of the FAO-56 θ_{crit} range. One possible explanation is that at the RO site, there were few cases of water-limited conditions. Although θ_{crit} values could be determined, rET_0 did not decrease significantly for SM values below θ_{crit} (Fig. S2 in Supplementary Material 2). In contrast, the SEro lysimeter observations showed a clear transition between water-limited and energy-limited regimes (Fig. S4 in Supplementary Material 2).

4. Discussion

Lysimeters provide a reliable means of quantifying in situ ET_a and are widely recognized as the gold standard, while also enabling SM measurements across different depths (Pütz & Groh, 2023). In this study, we applied θ_{crit} detection algorithms to a large dataset with lysimeter observations across Germany, not previously used for this purpose, and identified relationships between SM and ET_a.

We identified θ_{crit} not only from the EF-SM relationship, but also from rET_0 and $rPET_{FAO}$ definitions. The differences in lysimeter-specific θ_{crit} between the three definitions are small (Fig. 7), suggesting that any of them can be used to identify θ_{crit}, and that studies using these different definitions can be compared. However, the rET_0 definition led to a generally higher identification of θ_{crit} values (surface: 47, root zone: 49) with the lysimeters compared to the EF (surface: 38, root zone: 35) or $rPET_{FAO}$ definition (surface: 30, root zone: 33, Table 4). The higher number of θcrit detections for rET_0 was due to the relative simpler methodology used for ET_0, which yielded more data points compared to EF and $rPET_{FAO}$. A by-product of our analysis is the sensitivity of soil heat flux correction using calorimetric definitions, showing robustness despite varying inputs and soil parameters (Supplementary Material 1).

Although theoretically PET should be equal to ET_a in the energy-limited regime, the plateau values for both rET_0 and $rPET_{FAO}$ definitions fluctuated around 1 (Fig. 13). This discrepancy is understandable because the length of mid-season stage is estimated based on sowing and harvest dates, and the crop coefficients (K_c) for each crop are assumed to be constant based on FAO-56 guidelines, so PET_{FAO} is not the exact PET, implying the information from FAO-56 differs from the local conditions. However, even when using the site-specific K_c, the plateau values still were not equal to 1. Due to the difficulty and complexity of estimating the exact PET, and the fact that θ_{crit} estimated from the rET_0 definition is consistent with that from the EF definition, we recommend the rET_0 definition rather than the $rPET_{FAO}$ definition.

We also tested the impact of the fitting curves on the estimation of θ_{crit}. Very few studies fitted the relationship between SM-EF (or SM-rPET) using curves other than the linear-plus-plateau model. Dirmeyer et al. (2000) used an arctangent function to fit the relationship between root zone soil wetness index and EF, but this approach is unable to pinpoint a clear turning point. In this study, we applied the spherical variogram fitting curve to identify the θ_{crit} for the first time. We found that both linear-plus-plateau fitting and spherical variogram fitting give consistent results (Fig. 8), suggesting that the θ_{crit} is robust. However, though the performance of spherical variogram fitting is similar to linear-plus-plateau fitting (Fig. 8c), the spherical variogram fitting produced a smoother curve in the water-limited regime, indicating a gradual shift in the dependence of EF (or rPET) on SM. This smoother curve is perhaps closer to the behavior in nature and could offer additional insights into changes in the SM-EF (or SM-rPET) relationship.

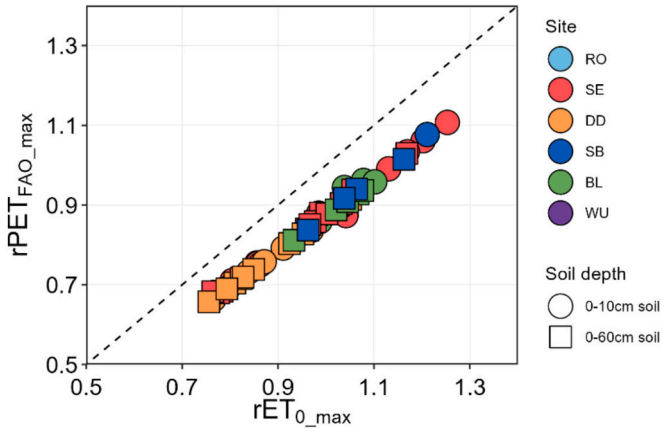

Fig. 13. Comparison between plateau values estimated from the rET_0 and $rPET_{FAO}$ definition across all the lysimeters. The dashed line is the 1:1 line.

Taking advantage of SM sensors installed at three different depths inside the lysimeters, our study estimates θ_{crit} for both surface and root zone soil. This is the advantage of the lysimeter data, as θ_{crit} for the root zone soil cannot be derived from satellite data (Purdy et al., 2018). It can be assumed that θ_{crit} estimated for the root zone is a better approximation of the true θ_{crit} as it captures better the SM control on the ET process, as also plant water uptake from deeper soil layers is considered. Plants take up water from roots, which can compensate for surface dryness and this water is transported from the deeper soil through the roots and stem to the transpiring leaves (Fan et al., 2017). Compared to the small uncertainty in θ_{crit} across different definitions and fitting curves as indicated by the low RMSD values, a much greater variability was observed in θ_{crit} between surface and root zone soil. Not surprisingly, our results show higher θ_{crit} for the root zone than for the surface

soil in Germany across different climatic regimes (semi-arid to humid regimes, Figs. 6 and 9), confirming results from Buitink et al. (2020) for the Netherlands and Dong et al. (2022) for the US.

While this study focused on SM, plants are known to be sensitive to water potentials, and it has been shown that the effective averaged soil water potential felt by a plant is proportional to its root distribution, when the soil hydraulic conductivity is not limiting water uptake (Couvreur et al., 2012). This implies that root spatial distribution should be used to weigh the soil water potential. However, because root spatial distribution is difficult to estimate (Zhang et al., 2023), computing an effective water potential as well as effective rootzone SM is very challenging.

We then made use of different lysimeter groups to investigate the dependence of θ_{crit} on soil texture. Some lysimeters at the same site have the same land use but different soils, allowing us to isolate the effect of soil texture without confounding factors. We find that both surface and root zone θ_{crit} decrease with increasing sand fraction (Fig. 10). Similar findings have been reported in previous studies, but only for surface soil without focusing on root zone soil (Denissen et al., 2020; Fu et al., 2024; Shi et al., 2024; Wankmüller et al., 2024). The slope of the fitted regression line for surface and sand fraction (−0.0011, Fig. 10a) is similar to that reported by Wankmüller et al. (2024), which is −0.0017. The underlying mechanism of the decreased θ_{crit} with increasing sand fraction can be attributed to the less negative matric potential in coarse-textured soils, which allows plants to access water at low water contents (Wankmüller et al., 2024). However, one limitation of this study is that we were not able to fully characterize θ_{crit} based on hydraulic conductivity due to limited soil texture information (only sand, silt and clay fractions were available for all lysimeters). Soil hydraulic conductivity is intrinsically dependent on soil particle size distribution (PSD) and can be estimated from empirical equations based on PSD (Wang et al., 2017). Further analysis can be carried out in more detail by exploring the relationship between θ_{crit} and hydraulic conductivity, or some indices related to PSD.

We also found that under the same climatic condition, sand fraction had a relatively minor impact on root zone θ_{crit} compared to surface θ_{crit} in arable land, whereas the opposite pattern was observed for grassland. One possible reason for this difference can be due to variations in root system density. Grasslands typically develop denser root systems over time, as their roots grow and persist year after year. In contrast, crops are replanted annually, resulting in less dense root systems (Dupont et al., 2014). This high root density increases water uptake from the root zone, making the root zone θ_{crit} more sensitive to changes in soil properties, such as sand fractions. However, there are not enough data points to show that the differences in slope between surface θ_{crit} and root zone θ_{crit} for arable land on one hand and grassland on the other hand were statistically significant.

The FAO-56 guidelines propose to estimate θ_{crit} for root zone soil (θ_{crit_FAO}) as the midpoint of field capacity and wilting point for a given soil texture. The comparison between root zone θ_{crit} estimated from lysimeter time series with θ_{crit_FAO} shows that the FAO-56 provides a generally reliable range of θ_{crit} for the four soil textures (sandy loam, loam, silt loam, sandy clay loam). However, for sandy clay loam, lysimeter-specific θ_{crit} at the RO site were mostly higher than the range of θ_{crit_FAO}. This is probably due to the few cases of water-limited conditions observed at the RO site. Although the fitting curves were able to determine θ_{crit}, there was no clear decrease in rET_0 or EF when SM decreased below θ_{crit} for most of the lysimeters at the RO site (Fig. S2 in Supplementary Material 2). It is important to note, however, that even a small decrease in EF can correspond to a substantial change in ET_a, particularly under high net radiation conditions. This warrants the need for further investigation into net radiation dynamics during soil dry-down events. Overall, the general agreement between FAO-56 and curve-fitting estimates of θ_{crit} highlights the potential for the FAO-56 and the curve fitting framework to serve as complementary methods for the estimation of θ_{crit}. The FAO-56 offers a broad yet reliable range of θ_{crit}, while the framework estimates the specific values. By combining the two methods, it is possible to cross-validate the results to obtain a more robust assessment of θ_{crit} for specific soil textures. Further study is needed to extend the analysis to a wider range of soil textures.

The impact of changing climatic conditions on θ_{crit} was examined using translocated lysimeters following the "space-for-time" concept. These lysimeters, some containing the same soil and vegetation types, were moved to sites with varying climatic conditions. We found that both surface and root zone θ_{crit} decrease with increasing aridity index (Fig. 11). We argue that atmospheric demand and plants play a competitive role on θ_{crit}. For drier conditions with higher evaporative demand, θ_{crit} should increase as soil water conductivity will become limiting at higher SM level; in other words, water limitation would be reached while the soil is still relatively wet during drying (Feldman et al., 2019; Carminati & Javaux, 2020). Thus, the observed decrease in θ_{crit} would suggest an overcompensation by vegetation, by increasing their root length, growing roots towards wetter zones or, for grassland, changing its composition towards more drought-tolerant plant species. However, due to the limited number of lysimeters, the changes in θ_{crit} due to the aridity index are not significant, suggesting that more data is needed to fully understand the impact of these factors.

In general a high correlation (0.83, Fig. 9a) was found between θ_{crit} for surface soil (10 cm) and for root zone soil (0–60 cm) in our study for the sites in Germany, ranging from semi-arid to humid regions. This correlation is higher than the value of 0.53 reported by Dong et al. (2022), who compared surface θ_{crit} (5 cm) and root zone θ_{crit} (0–50 cm) using AmeriFlux data from the continental United States. Furthermore, this correlation is in line with a recent global study using ERA5 reanalysis data (Paul et al., 2025). They found a correlation of 0.86 between surface θ_{crit} (0–7 cm) and shallow root zone θ_{crit} (0–28 cm) and a lower correlation of 0.74 between surface θ_{crit} and deeper root zone θ_{crit} (0–100 cm). Interestingly, although our results only focused on 6 sites in Germany, which are fewer and with a narrower climatic gradient compared to Dong et al. (2022), we find a similar range of θ_{crit} (0.1 ~ 0.35 m^3/m^3), indicating that our sites are representative of some typical climate types. The high correlation between surface θ_{crit} and root zone θ_{crit} can be explained by the hydraulic link that governs water movement and distribution within the soil profile, suggesting both surface and root zone SM can capture comparable statistics of ET_a regime prevalence (Dong et al., 2022). However, it is worth noting that regions which may have abrupt dry and wet seasons, such as the Indian and East African Summer Monsoons (Mondal & Mishra, 2024), may exhibit much larger discrepancies in θ_{crit} between surface and root zone SM and poor correlations between them. Under those conditions surface and root zone SM sometimes decouple with a very dry surface soil layer and still relatively elevated SM in the deeper root zone (Capehart & Carlson, 1997; Vereecken et al., 2008). In those cases, or for arid sites θ_{crit} estimated from the upper SM would not be very representative of θ_{crit}. For example, Paul et al (2025) found a greater difference between surface and root zone θ_{crit} in drier ecosystems (savannas and shrublands) than in wetter woody vegetation regions. This highlights the need for further investigation for different climate conditions, like arid and monsoon type climates.

In addition, the apparent rooting depths exhibit a broad range (even up to 25 m) across the globe (Stocker et al., 2023). We estimated root zone SM for the upper 60 cm, which might not be representative of the complete effective rooting zone. Future studies should incorporate deeper soil layers to better capture root zone SM and hence root zone θ_{crit}.

Our findings also have broader implications for the remote sensing and land surface modeling communities. Many remotely sensed products of ET_a and model-derived ET_a estimates tend to perform better under energy-limited conditions (Long et al., 2014). By providing observationally constrained estimates of θ_{crit}, our findings indicate that lysimeter-derived θ_{crit} offers possibilities to delineate ET_a regimes and identify the areas where specific remote sensing products or model

simulations are expected to perform more reliably. Moreover, the lysimeter-based quantification of θ_{crit} provides valuable reference data for validating and improving the models and remote sensing products, contributing to a better understanding of land–atmosphere coupling processes under changing climatic conditions.

5. Conclusions

We provide estimates of critical soil moisture thresholds (θ_{crit}), the soil moisture content at which the transition from energy limited to water limited ET_a occurs, for both surface (10 cm) and root zone (0–60 cm) soil based on lysimeter data sets. Lysimeters are considered the gold standard for measuring in situ ET_a and allow concurrent in situ SM measurements at various depths. A total of 61 lysimeters from 7 sites in Germany were employed for this analysis including different soil texture and land cover types (grassland and arable land). The relationships between SM and evaporative fraction (EF), SM and the ratio of actual evapotranspiration to grass reference evapotranspiration (rET_0), and SM and the ratio of actual evapotranspiration to calculated potential evapotranspiration ($rPET_{FAO}$) during drydowns were fitted by a linear plus plateau function and a spherical variogram function to determine θ_{crit}. All three definitions and two fitting functions showed good consistency, indicating the applicability of each of the three definitions or the two fitting curve frameworks. The root zone θ_{crit} was found to be higher than surface θ_{crit}. θ_{crit} for both surface and root zone soil showed a dependency on sand fraction ($R^2 = 0.38$ for surface θ_{crit} and $R^2 = 0.16$ for root zone θ_{crit}). In addition, under changing climatic conditions but with identical soil and ecosystem, θ_{crit} increased when the soil monoliths moved to a drier place with higher aridity index. Overall, θ_{crit} showed a dependence on aridity index ($R^2 = 0.12$ for surface θ_{crit} and $R^2 = 0.23$ for root zone θ_{crit}). Although the difference between surface and root-zone based θ_{crit} was greater than between any of the abovementioned definitions, and cannot be ignored, we still found a good correlation between surface soil and root zone θ_{crit}. Consequently, while θ_{crit} from different measurement depths (i.e., surface vs. root zone layers) should not be directly compared, they might still serve as mutual proxies. However, we argue that it can be expected that for other climates (monsoon, arid) and (very) deep rooting vegetation this correlation may break down. This warrants further investigation with in-situ data for those sites.

CRediT authorship contribution statement

Xiao Lu: Writing – review & editing, Writing – original draft, Visualization, Methodology, Funding acquisition, Formal analysis, Data curation, Conceptualization. **Jannis Groh:** Writing – review & editing, Methodology, Formal analysis, Data curation, Conceptualization. **Alexander Graf:** Writing – review & editing, Methodology, Formal analysis, Data curation, Conceptualization. **Thomas Pütz:** Writing – review & editing, Data curation. **Horst H. Gerke:** Writing – review & editing, Data curation. **Ralf Gründling:** Writing – review & editing, Data curation. **Holger Rupp:** Writing – review & editing, Data curation. **Ralf Kiese:** Writing – review & editing, Data curation. **Hans Jörg Vogel:** Writing – review & editing, Data curation. **Mathieu Javaux:** Writing – review & editing, Methodology. **Harry Vereecken:** Writing – review & editing, Methodology, Formal analysis, Conceptualization. **Harrie-Jan Hendricks Franssen:** Writing – review & editing, Supervision, Methodology, Formal analysis, Conceptualization.

Declaration of competing interest

The authors declare that they have no known competing financial interests or personal relationships that could have appeared to influence the work reported in this paper.

Acknowledgements

This work is funded by the China Scholarship Council (CSC), Grant: 202006710010. We acknowledge the support of TERENO and SOILCan, which were funded by the Helmholtz Association (HGF) and the Federal Ministry of Education and Research (BMBF). Jannis Groh is funded by the Deutsche Forschungsgemeinschaft (DFG, German Research Foundation) –project no. 460817082. We thank the colleagues at the corresponding lysimeter stations for their kind support: Rainer Gasche and Ingo Völksch (Graswang) and Werner Küpper, Ferdinand Engels, Philipp Meulendick, Rainer Harms, Leander Fürst, Daniel Dolfus, Nils Becker, Martina Kettler and Marius Schmidt (Rollesbroich, Selhausen, and Wüstebach), Jörg Haase, Gernot Verch (Dedelow), Sylvia Schmögner, Robert Lüdtke, Ralf Gründling (Bad Lauchstädt, Sauerbach).

We wish to thank Jan Vanderborght (IBG-3, Forschungszentrum Jülich, Germany) who provided inspirational discussions and skilled suggestions on the topic.

Appendix A. Supplementary data

Supplementary data to this article can be found online at https://doi.org/10.1016/j.jhydrol.2026.134959.

Data availability

The weather, soil moisture and lysimeter data (raw data) for Rollesbroich (RO), Wüstebach (WU) and Selhausen (SE) sites can be freely obtained from the TERENO data portal (https://teodoor.icg.kfa-juelich.de/ddp/index.jsp). The short names of the weather station IDs are ro_bky_010 for the RO site, wu_bky_010 for the WU site and se_bk_001 for the SE site. The soil moisture and lysimeter data are available for the lysimeters whose short names are ro_y_011 to ro_y_016 for the RO site, wu_y_011 to wu_y_016 for the WU site and se_y_011 to se_y_046 for the SE site. The quality of the data used in this study is classified as “Good”.

The data for the sites Dedelow (DD), Sauerbach (SB), Bad-Lauchstädt (BL) and Graswang (GW), as well as the processed data during this study can be acquired upon request.

References

Akaike, H., 1974. A new look at the statistical model identification. IEEE Trans. Autom. Control 19 (6), 716–723. https://doi.org/10.1109/TAC.1974.1100705.

Akbar, R., Gianotti, D.J.S., McColl, K.A., Haghighi, E., Salvucci, G.D., Entekhabi, D., 2018. Estimation of landscape soil water losses from satellite observations of soil moisture. J. Hydrometeorol. 19 (5), 871–889 https://doi.org/fi.

Allen, R.G., Pereira, L.S., Raes, D., Smith, M., et al., 1998. Crop evapotranspiration-guidelines for computing crop water requirements-FAO Irrigation and drainage paper 56. Fao, Rome 300 (9), D05109.

Allen, R.G., Pruitt, W.O., Wright, J.L., Howell, T.A., Ventura, F., Snyder, R., Itenfisu, D., Steduto, P., Berengena, J., Yrisarry, J.B., Smith, M., Pereira, L.S., Raes, D., Perrier, A., Alves, I., Walter, I., Elliott, R., 2006. A recommendation on standardized surface resistance for hourly calculation of reference ETo by the FAO56 Penman-Monteith method. Agric Water Manag 81 (1–2), 1–22. https://doi.org/10.1016/j.agwat.2005.03.007.

Berg, A., Findell, K., Lintner, B., Giannini, A., Seneviratne, S.I., Van Den Hurk, B., Lorenz, R., Pitman, A., Hagemann, S., Meier, A., Cheruy, F., Ducharne, A., Malyshev, S., Milly, P.C.D., 2016. Land-atmosphere feedbacks amplify aridity increase over land under global warming. Nat. Clim. Chang. 6 (9), 869–874. https://doi.org/10.1038/nclimate3029.

Blois, J.L., Williams, J.W., Fitzpatrick, M.C., Jackson, S.T., Ferrier, S., 2013. Space can substitute for time in predicting climate-change effects on biodiversity. PNAS 110 (23), 9374–9379. https://doi.org/10.1073/pnas.1220228110.

Brown, W.G., Cosh, M.H., Dong, J., Ochsner, T.E., 2023. Upscaling soil moisture from point scale to field scale: Toward a general model. Vadose Zone J. 22 (2), 1–14. https://doi.org/10.1002/vzj2.20244.

Budyko, M. I. (1974). Climate and life.

Buitink, J., Swank, A.M., Van Der Ploeg, M., Smith, N.E., Benninga, H.J.F., Van Der Bolt, F., Carranza, C.D.U., Koren, G., Van Der Velde, R., Teuling, A.J., 2020. Anatomy of the 2018 agricultural drought in the Netherlands using in situ soil moisture and satellite vegetation indices. Hydrol. Earth Syst. Sci. 24 (12), 6021–6031. https://doi.org/10.5194/hess-24-6021-2020.

Capehart, W.J., Carlson, T.N., 1997. Decoupling of surface and near-surface soil water content: a remote sensing perspective. Water Resour. Res. 33 (6), 1383–1395.

Carminati, A., Javaux, M., 2020. Soil rather than xylem vulnerability controls stomatal response to drought. Trends Plant Sci. 25 (9), 868–880. https://doi.org/10.1016/j.tplants.2020.04.003.

Chu, H., Luo, X., Ouyang, Z., Chan, W.S., Dengel, S., Biraud, S.C., Torn, M.S., Metzger, S., Kumar, J., Arain, M.A., Arkebauer, T.J., Baldocchi, D., Bernacchi, C., Billesbach, D., Black, T.A., Blanken, P.D., Bohrer, G., Bracho, R., Brown, S., Zona, D., 2021. Representativeness of Eddy-Covariance flux footprints for areas surrounding AmeriFlux sites. Agric. For. Meteorol. 301–302, 108350. https://doi.org/10.1016/J.AGRFORMET.2021.108350.

Corami, A., Eslamian, S., & Eslamian, F. (2024). Fundamentals of Evapotranspiration. Taylor and Francis, CRC Group, USA. https://doi.org/10.1201/9781003467229.

Couvreur, V., Vanderborght, J., Javaux, M., 2012. A simple three-dimensional macroscopic root water uptake model based on the hydraulic architecture approach. Hydrol. Earth Syst. Sci. 16 (8), 2957–2971. https://doi.org/10.5194/hess-16-2957-2012.

Denissen, J.M.C., Teuling, A.J., Reichstein, M., Orth, R., 2020. Critical soil moisture derived from satellite observations over Europe. J. Geophys. Res. Atmos. 125 (6), 1–10. https://doi.org/10.1029/2019JD031672.

Ding, R., Kang, S., Li, F., Zhang, Y., Tong, L., Sun, Q., 2010. Evaluating eddy covariance method by large-scale weighing lysimeter in a maize field of northwest China. Agric Water Manag 98 (1), 87–95. https://doi.org/10.1016/j.agwat.2010.08.001.

Dirmeyer, P.A., Zeng, F.J., Ducharne, A., Morrill, J.C., Koster, R.D., 2000. The sensitivity of surface fluxes to soil water content in three land surface schemes. J. Hydrometeorol. 1 (2), 121–134. https://doi.org/10.1175/1525-7541(2000)001<0121:TSOSFT>2.0.CO;2.

Dong, J., Akbar, R., Feldman, A.F., Gianotti, D.S., Entekhabi, D., 2023. Land surfaces at the tipping-point for water and energy balance coupling. Water Resour. Res. 59 (2), 1–15. https://doi.org/10.1029/2022WR032472.

Dong, J., Akbar, R., Short Gianotti, D.J., Feldman, A.F., Crow, W.T., Entekhabi, D., 2022. Can surface soil moisture information identify evapotranspiration regime transitions? Geophys. Res. Lett. 49 (7). https://doi.org/10.1029/2021GL097697.

Dupont, S. T., Beniston, J., Glover, J. D., & Hodson, A. (2014). Root traits and soil properties in harvested perennial grassland, annual wheat , and never-tilled annual wheat. 405–420. https://doi.org/10.1007/s11104-014-2145-2.

Eagleson, P.S., 1978. Climate, soil, and vegetation: 4. the expected value of annual evapotranspiration. Water Resour. Res. 14 (5), 731–739. https://doi.org/10.1029/WR014i005p00731.

Elzhov, T. V, Mullen, K. M., Spiess, A.-N., & Bolker, B. (2015). minpack. lm: R interface to the Levenberg-Marquardt nonlinear least-squares algorithm found in MINPACK, plus support for bounds. R package version 1.1-8. CRAN. R-Project. Org/Package= Minpack. Lm.

Escorihuela, M.J., Chanzy, A., Wigneron, J.P., Kerr, Y.H., 2010. Remote Sensing of Environment Effective soil moisture sampling depth of L-band radiometry: a case study. Remote Sens. Environ. 114 (5), 995–1001. https://doi.org/10.1016/j.rse.2009.12.011.

Fan, Y., Miguez-Macho, G., Jobbágy, E.G., Jackson, R.B., Otero-Casal, C., 2017. Hydrologic regulation of plant rooting depth. PNAS 114 (40), 10572–10577. https://doi.org/10.1073/pnas.1712381114.

Feldman, A.F., Short Gianotti, D.J., Trigo, I.F., Salvucci, G.D., Entekhabi, D., 2019. Satellite-based assessment of land surface energy partitioning–soil moisture relationships and effects of confounding variables. Water Resour. Res. 55 (12), 10657–10677. https://doi.org/10.1029/2019WR025874.

Fisher, J.B., Melton, F., Middleton, E., Hain, C., Anderson, M., Allen, R., McCabe, M.F., Hook, S., Baldocchi, D., Townsend, P.A., Kilic, A., Tu, K., Miralles, D.D., Perret, J., Lagouarde, J.P., Waliser, D., Purdy, A.J., French, A., Schimel, D., Wood, E.F., 2017. The future of evapotranspiration: Global requirements for ecosystem functioning, carbon and climate feedbacks, agricultural management, and water resources. Water Resour. Res. 53 (4), 2618–2626. https://doi.org/10.1002/2016WR020175.

Ford, T.W., Harris, E., Quiring, S.M., 2014a. Estimating root zone soil moisture using near-surface observations from SMOS. Hydrol. Earth Syst. Sci. 1994, 139–154. https://doi.org/10.5194/hess-18-139-2014.

Ford, T.W., Wulff, C.O., Quiring, S.M., 2014b. Assessment of observed and model-derived soil moisture-evaporative fraction relationships over the United States southern great plains. J. Geophys. Res. 119 (11), 6279–6291. https://doi.org/10.1002/2014JD021490.

Franssen, H.J.H., Stöckli, R., Lehner, I., Rotenberg, E., Seneviratne, S.I., 2010. Energy balance closure of eddy-covariance data : a multisite analysis for European FLUXNET stations. Agric. For. Meteorol. https://doi.org/10.1016/j.agrformet.2010.08.005.

Fu, Z., Ciais, P., Feldman, A.F., Gentine, P., Makowski, D., Prentice, I.C., Stoy, P.C., Bastos, A., Wigneron, J.P., 2022. Critical soil moisture thresholds of plant water stress in terrestrial ecosystems. Sci. Adv. 8 (44), 1–13. https://doi.org/10.1126/sciadv.abq7827.

Fu, Z., Ciais, P., Wigneron, J.-P., Gentine, P., Andrew F. Feldman, Makowski, D., Viovy, N., Kemanian, A. R., DanielS.Goll, PaulC.Stoy, Prentice, I., Yakir, D., Liu, L., Ma, H., Li, X., Huang, Y., Yu, K., Zhu, P., Li, X., … Smith, W. K. (2024). Global critical soil moisture thresholds of plant water stress. Nature Communications, 22 May 2024, 5194. https://doi.org/10.1038/s41467-024-49244-7.

Gao, Z., Russell, E.S., Missik, J.E.C., Huang, M., Chen, X., Strickland, C.E., Clayton, R., Arntzen, E., Ma, Y., Liu, H., 2017. A novel approach to evaluate soil heat flux calculation: an analytical review of nine methods. J. Geophys. Res. 122 (13), 6934–6949. https://doi.org/10.1002/2017JD027160.

Gebler, S., Hendricks Franssen, H.J., Pütz, T., Post, H., Schmidt, M., Vereecken, H., 2015. Actual evapotranspiration and precipitation measured by lysimeters: a comparison with eddy covariance and tipping bucket. Hydrol. Earth Syst. Sci. 19 (5), 2145–2161. https://doi.org/10.5194/hess-19-2145-2015.

Giambelluca, T.W., Scholz, F.G., Bucci, S.J., Meinzer, F.C., Goldstein, G., Hoffmann, W. A., Franco, A.C., Buchert, M.P., 2009. Evapotranspiration and energy balance of Brazilian savannas with contrasting tree density. Agric. For. Meteorol. 149 (8), 1365–1376. https://doi.org/10.1016/j.agrformet.2009.03.006.

Giraud, M., Groh, J., Gerke, H.H., Brüggemann, N., Vereecken, H., Pütz, T., 2021. Soil nitrogen dynamics in a managed temperate grassland under changed climatic conditions. Water 1–23.

Green, J.K., Zhang, Y., Luo, X., Keenan, T.F., 2024. Systematic underestimation of canopy conductance sensitivity to drought by earth system models. AGU Adv. 5 (1). https://doi.org/10.1029/2023AV001026.

Groh, J., Diamantopoulos, E., Duan, X., Ewert, F., Heinlein, F., Herbst, M., Holbak, M., Kamali, B., Kersebaum, K.C., Kuhnert, M., Nendel, C., Priesack, E., Steidl, J., Sommer, M., Pütz, T., Vanderborght, J., Vereecken, H., Wallor, E., Weber, T.K.D., Gerke, H.H., 2022. Same soil, different climate: crop model intercomparison on translocated lysimeters. Vadose Zone J. 21 (4), 1–25. https://doi.org/10.1002/vzj2.20202.

Groh, J., Diamantopoulos, E., Duan, X., Ewert, F., Herbst, M., Holbak, M., Kamali, B., Kersebaum, K.-C., Kuhnert, M., Lischeid, G., et al., 2020a. Crop growth and soil water fluxes at erosion-affected arable sites: using weighing lysimeter data for model intercomparison. Vadose Zone J. 19 (1), e20058.

Groh, J., Pütz, T., Gerke, H.H., Vanderborght, J., Vereecken, H., 2019. Quantification and prediction of nighttime evapotranspiration for two distinct grassland ecosystems. Water Resour. Res. 55 (4), 2961–2975. https://doi.org/10.1029/2018WR024072.

Groh, J., Vanderborght, J., Pütz, T., Gründling, R., Rupp, H., Rahmati, M., Sommer, M., Sommer, M., Vereecken, H., Gerke, H.H., 2020b. Responses of soil water storage and crop water use efficiency to changing climatic conditions: a lysimeter-based space-for-time approach. Hydrol. Earth Syst. Sci. 24 (3), 1211–1225. https://doi.org/10.5194/hess-24-1211-2020.

Groh, J., Vanderborght, J., Pütz, T., Vereecken, H., 2016. How to control the lysimeter bottom boundary to investigate the effect of climate change on soil processes? Vadose Zone J. 15 (7), vzj2015.08.0113. https://doi.org/10.2136/vzj2015.08.0113.

Haghighi, E., Short Gianotti, D. J., Akbar, R., Salvucci, G. D., & Entekhabi, D. (2018). Soil and Atmospheric Controls on the Land Surface Energy Balance: A Generalized Framework for Distinguishing Moisture-Limited and Energy-Limited Evaporation Regimes. 1831–1851. https://doi.org/10.1002/2017WR021729.

Hirschi, M., Michel, D., Lehner, I., Seneviratne, S.I., 2017. A site-level comparison of lysimeter and eddy covariance flux measurements of evapotranspiration. Hydrol. Earth Syst. Sci. 21 (3), 1809–1825. https://doi.org/10.5194/hess-21-1809-2017.

Hirschi, M., Mueller, B., Dorigo, W., Seneviratne, S.I., 2014. Using remotely sensed soil moisture for land – atmosphere coupling diagnostics: the role of surface vs. root-zone soil moisture variabilit. Remote Sens. Environ. 154, 246–252. https://doi.org/10.1016/j.rse.2014.08.030.

Hsu, H., Dirmeyer, P.A., 2023a. Soil moisture-evaporation coupling shifts into new gears under increasing CO2. Nat. Commun. 14 (1). https://doi.org/10.1038/s41467-023-36794-5.

Hsu, H., Dirmeyer, P.A., 2023b. Uncertainty in projected critical soil moisture values in CMIP6 affects the interpretation of a more moisture-limited world. Earth's Future 11 (6), 1–15. https://doi.org/10.1029/2023ef003511.

Humphrey, V., Berg, A., Ciais, P., Gentine, P., Jung, M., Reichstein, M., Seneviratne, S.I., Frankenberg, C., 2021. Soil moisture – atmosphere feedback dominates land carbon uptake variability. Nature 592 (April). https://doi.org/10.1038/s41586-021-03325-5.

Iwema, J., Rosolem, R., Rahman, M., Blyth, E., Wagener, T., 2017. Land surface model performance using cosmic-ray and point-scale soil moisture measurements for calibration. Hydrol. Earth Syst. Sci. 21 (6), 2843–2861. https://doi.org/10.5194/hess-21-2843-2017.

Jarvis, N., Groh, J., Lewan, E., Meurer, K.H.E., Durka, W., Baessler, C., Pütz, T., Rufullayev, E., Vereecken, H., 2022. Coupled modelling of hydrological processes and grassland production in two contrasting climates. Hydrol. Earth Syst. Sci. 26 (8), 2277–2299. https://doi.org/10.5194/hess-26-2277-2022.

Kauwe, M. G. De, Medlyn, B. E., Knauer, J., & Williams, C. A. (2017). Ideas and perspectives : how coupled is the vegetation to the boundary layer ? 4435–4453.

Kiese, R., Fersch, B., Baessler, C., Brosy, C., Butterbach-Bahl, K., Chwala, C., Dannenmann, M., Fu, J., Gasche, R., Grote, R., Jahn, C., Klatt, J., Kunstmann, H., Mauder, M., Rödiger, T., Smiatek, G., Soltani, M., Steinbrecher, R., Völksch, I., Schmid, H.P., 2018. The TERENO pre-alpine observatory: integrating meteorological, hydrological, and biogeochemical measurements and modeling. Vadose Zone J. 17 (1), 180060. https://doi.org/10.2136/vzj2018.03.0060.

Koster, R.D., Feldman, A.F., Holmes, T.R.H., Anderson, M.C., Crow, W.T., Hain, C., 2024. Estimating hydrological regimes from observational soil moisture, evapotranspiration, and air temperature Da. J. Hydrometeorol. 495–513. https://doi.org/10.1175/JHM-D-23-0140.1.

Koster, R.D., Schubert, S.D., Suarez, M.J., 2009. Analyzing the concurrence of meteorological droughts and warm periods, with implications for the determination of evaporative regime. J. Clim. 22 (12), 3331–3341. https://doi.org/10.1175/2008JCLI2718.1.

Li, W., Hendricks Franssen, H. J., Brunner, P., Li, Z., Wang, Z., Wang, Y., & Wang, W. (2022). The role of soil texture on diurnal and seasonal cycles of potential evaporation over saturated bare soils – Lysimeter studies. Journal of Hydrology, 613 (December 2021). https://doi.org/10.1016/j.jhydrol.2022.128194.

Liu, Y., Xiao, J., Li, X., Li, Y., 2024. Critical soil moisture detection and water-energy limit shift attribution using satellite-based water and carbon fluxes over China. Hydrol. Earth Syst. Sci. 1–30.

Lo, M.H., Wu, W.Y., Tang, L.I., Ryu, D., Rashid, M., Wu, R.J., 2021. Temporal changes in land surface coupling strength: an example in a semi-arid region of Australia. J. Clim. 34 (4), 1503–1513. https://doi.org/10.1175/JCLI-D-20-0250.1.

Lu, X., Groh, J., Graf, A., Pütz, T., Schneider, K., Si, B., Vereecken, H., Franssen, H.J.H., 2024. Analysis of scale-dependent spatial correlations of actual evapotranspiration measured by lysimeters. Agric. For. Meteorol. 359 (October), 110288. https://doi.org/10.1016/j.agrformet.2024.110288.

Mahmood, R., & Hubbard, K. G. (2007). Relationship between soil moisture of near surface and multiple depths of the root zone under heterogeneous land uses and varying hydroclimatic conditions. 3462(July), 3449–3462. https://doi.org/10.1002/hyp.

Mälicke, M., Hassler, S. K., Weiler, M., Blume, T., & Zehe, E. (2018). Exploring hydrological similarity during soil moisture recession periods using time dependent variograms. September, 1–25.

Manabe, S., 1969. Climate and the ocean circulation: the atmospheric circulation and the hydrology of the earth's surface. Mon. Weather Rev. 97 (11), 739–774. http://journals.ametsoc.org/doi/abs/10.1175/1520-0493(1969)097%3C0739:CATOC%3E2.3.CO;2.

Martens, B., Miralles, D.G., Lievens, H., Van Der Schalie, R., De Jeu, R.A.M., Fernández-Prieto, D., Beck, H.E., Dorigo, W.A., Verhoest, N.E.C., 2017. GLEAM v3: Satellite-based land evaporation and root-zone soil moisture. Geosci. Model Dev. 10 (5), 1903–1925. https://doi.org/10.5194/gmd-10-1903-2017.

Mauder, M., Ibrom, A., Wanner, L., Roo, F. De, Brugger, P., & Kiese, R. (2021). Options to correct local turbulent flux measurements for large-scale fluxes using an approach based on large-eddy simulation. 7835–7850.

McColl, K.A., Wang, W., Peng, B., Akbar, R., Short Gianotti, D.J., Lu, H., Pan, M., Entekhabi, D., 2017. Global characterization of surface soil moisture drydowns. Geophys. Res. Lett. 44 (8), 3682–3690. https://doi.org/10.1002/2017GL072819.

Mondal, S., Mishra, A., 2024. Quantifying the precipitation, evapotranspiration, and soil moisture network's interaction over global land surface hydrological cycle. Water Resour. Res. 60 (2). https://doi.org/10.1029/2023WR034861.

Oliveira, R.S., Davidson, E.A., Klink, C.A., Moreira, A., 2005. Deep root function in soil water dynamics in cerrado savannas of central Brazil. Funct. Ecol. 1996, 574–581. https://doi.org/10.1111/j.1365-2435.2005.01003.x.

Oliver, M. A., Webster, R., & others. (2015). Basic steps in geostatistics: the variogram and kriging.

Paul, S., Feldman, A.F., Karthikeyan, L., 2025. Are rootzone soil moisture dynamics and thresholds associated with surface layer? Environ. Res. Lett. 20 (1), 014037. https://doi.org/10.1088/1748-9326/ad9293.

Peng, L., Zeng, Z., Wei, Z., Chen, A., Wood, E.F., Sheffield, J., 2019. Determinants of the ratio of actual to potential evapotranspiration. Glob. Chang. Biol. 25 (4), 1326–1343. https://doi.org/10.1111/gcb.14577.

Peters, A., Groh, J., Schrader, F., Durner, W., Vereecken, H., Pütz, T., 2017. Towards an unbiased filter routine to determine precipitation and evapotranspiration from high precision lysimeter measurements. J. Hydrol. 549, 731–740. https://doi.org/10.1016/j.jhydrol.2017.04.015.

Peters, A., Nehls, T., Schonsky, H., Wessolek, G., 2014. Separating precipitation and evapotranspiration from noise – a new filter routine for high-resolution lysimeter data. Hydrol. Earth Syst. Sci. 18 (3), 1189–1198. https://doi.org/10.5194/hess-18-1189-2014.

Purdy, A.J., Fisher, J.B., Goulden, M.L., Colliander, A., Halverson, G., Tu, K., Famiglietti, J.S., 2018. SMAP soil moisture improves global evapotranspiration. Remote Sens. Environ. 219 (October), 1–14. https://doi.org/10.1016/j.rse.2018.09.023.

Pütz, T., Groh, J. (2023). Lysimetry. In M. J. Goss & M. Oliver (Eds.), Encyclopedia of Soils in the Environment (Second Edition) (Second Edition, pp. 667–679). Academic Press. https://doi.org/10.1016/B978-0-12-822974-3.00272-X.

Pütz, T., Kiese, R., Wollschläger, U., Groh, J., Rupp, H., Zacharias, S., Priesack, E., Gerke, H.H., Gasche, R., Bens, O., Borg, E., Baessler, C., Kaiser, K., Herbrich, M., Munch, J.-C., Sommer, M., Vogel, H.-J., Vanderborght, J., Vereecken, H., 2016. TERENO-SOILCan: a lysimeter-network in Germany observing soil processes and plant diversity influenced by climate change. Environ. Earth Sci. 75 (18), 1242. https://doi.org/10.1007/s12665-016-6031-5.

Qiu, J., Crow, W.T., Dong, J., Nearing, G.S., 2020. Model representation of the coupling between evapotranspiration and soil water content at different depths. Hydrol. Earth Syst. Sci. 24 (2), 581–594. https://doi.org/10.5194/hess-24-581-2020.

Qiu, J., Crow, W.T., Nearing, G.S., 2016. The impact of vertical measurement depth on the information content of soil moisture for latent heat flux estimation. J. Hydrometeorol. 17 (9), 2419–2430. https://doi.org/10.1175/JHM-D-16-0044.1.

Raes, D., Steduto, P., Hsiao, T. C., & Fereres, E. (2023). Chapter 2: Users guide. AquaCrop version 7.1. Reference Manual. Food and Agriculture Organization of the United Nations Rome, August.

Schneider, J., Groh, J., Pütz, T., Helmig, R., Rothfuss, Y., Vereecken, H., Vanderborght, J., 2021. Prediction of soil evaporation measured with weighable lysimeters using the FAO Penman–Monteith method in combination with Richards' equation. Vadose Zone J. 20 (1), 1–20. https://doi.org/10.1002/vzj2.20102.

Schrader, F., Durner, W., Fank, J., Gebler, S., Pütz, T., Hannes, M., Wollschläger, U., 2013. Estimating precipitation and actual evapotranspiration from precision lysimeter measurements. Procedia Environ. Sci. 19, 543–552. https://doi.org/10.1016/j.proenv.2013.06.061.

Schwingshackl, C., Hirschi, M., Seneviratne, S.I., 2017. Quantifying spatiotemporal variations of soil moisture control on surface energy balance and near-surface air temperature. J. Clim. 30 (18), 7105–7124. https://doi.org/10.1175/JCLI-D-16-0727.1.

Seneviratne, S.I., Corti, T., Davin, E.L., Hirschi, M., Jaeger, E.B., Lehner, I., Orlowsky, B., Teuling, A.J., 2010. Investigating soil moisture-climate interactions in a changing climate: a review. Earth Sci. Rev. 99 (3–4), 125–161. https://doi.org/10.1016/j.earscirev.2010.02.004.

Shellito, P.J., Small, E.E., Livneh, B., 2018. Controls on surface soil drying rates observed by SMAP and simulated by the Noah land surface model. Hydrol. Earth Syst. Sci. 22 (3), 1649–1663. https://doi.org/10.5194/hess-22-1649-2018.

Shi, L., Zhou, Y., He, W., Dong, Z., Jiang, Z., Wang, Y., Liu, Y., Ju, W., Duan, Z., 2024. Mapping critical soil moisture thresholds of water stress for global grasslands. J. Hydrol., 132090 https://doi.org/10.1016/j.jhydrol.2024.132090.

Sörensson, A.A., Ruscica, R.C., 2018. Intercomparison and uncertainty assessment of nine evapotranspiration estimates over South America. Water Resour. Res. 54 (4), 2891–2908. https://doi.org/10.1002/2017WR021682.

Stocker, B. D., Tumber-dávila, S. J., Konings, A. G., Anderson, M. C., Hain, C., Jackson, R. B., 2023. Global patterns of water storage in the rooting zones of vegetation. 16 (March). https://doi.org/10.1038/s41561-023-01125-2.

Thompson, S.E., Harman, C.J., Konings, A.G., Sivapalan, M., Neal, A., Troch, P.A., 2011. Comparative hydrology across AmeriFlux sites: the variable roles of climate, vegetation, and groundwater. Water Resour. Res. 47 (7), 1–17. https://doi.org/10.1029/2010WR009797.

Troch, P.A., Lahmers, T., Meira, A., Mukherjee, R., Pedersen, J.W., Roy, T., Valdés-Pineda, R., 2015. Catchment coevolution: a useful framework for improving predictions of hydrological change? Water Resour. Res. 51 (7), 4903–4922.

van Groenigen, J.W., 2000. The influence of variogram parameters on optimal sampling schemes for mapping by kriging. Geoderma 97 (3), 223–236. https://doi.org/10.1016/S0016-7061(00)00040-9.

Vereecken, H., Huisman, J.A., Bogena, H., Vanderborght, J., Vrugt;, J.A., Hopmans, J.W., 2008. On the value of soil moisture measurements in vadose zone hydrology: a review. Water Resour. Res. 46 (4), 1–21. https://doi.org/10.1029/2008WR006829.

Wadoux, A.-M.-C., Marchant, B.P., Lark, R.M., 2019. Efficient sampling for geostatistical surveys. Eur. J. Soil Sci. 70 (5), 975–989.

Wang, J., Franc, B., Lambert, P., 2017. Equations for hydraulic conductivity estimation from particle size distribution: a dimensional analysis. Water Resour. Res. https://doi.org/10.1002/2017WR020888.

Wang, K., Dickinson, R.E., 2012. A review of global terrestrial evapotranspiration: observation, modeling, climatology, and climatic variability. Rev. Geophys. 50 (2). https://doi.org/10.1029/2011RG000373.

Wankmüller, F.J.P., Delval, L., Lehmann, P., Baur, M.J., Cecere, A., Wolf, S., Or, D., Javaux, M., Carminati, A., 2024. Global influence of soil texture on ecosystem water limitation. Nature 635 (November). https://doi.org/10.1038/s41586-024-08089-2.

Widmoser, P., Wohlfahrt, G., 2018. Attributing the energy imbalance by concurrent lysimeter and eddy covariance evapotranspiration measurements. Agric. For. Meteorol. 263 (March), 287–291. https://doi.org/10.1016/j.agrformet.2018.09.003.

Xiang, K., Li, Y., Horton, R., Feng, H., 2020. Similarity and difference of potential evapotranspiration and reference crop evapotranspiration – a review. Agric Water Manag 232, 106043. https://doi.org/10.1016/J.AGWAT.2020.106043.

Yao, A.Y.M., 1974. Agricultural potential estimated from the ratio of actual to potential evapotranspiration. 3, 405–417.

Zacharias, S., Loescher, H.W., Bogena, H., Kiese, R., Schrön, M., Attinger, S., Blume, T., Borchardt, D., Borg, E., Bumberger, J., Chwala, C., Dietrich, P., Fersch, B., Frenzel, M., Gaillardet, J., Groh, J., Hajnsek, I., Itzerott, S., Kunkel, R., Vereecken, H., 2024. Fifteen years of integrated terrestrial environmental observatories (TERENO) in Germany: functions, services, and lessons learned. Earth's Future 12 (6), 1–30. https://doi.org/10.1029/2024EF004510.

Zhang, P., Jeong, J.H., Yoon, J.H., Kim, H., Simon Wang, S.Y., Linderholm, H.W., Fang, K., Wu, X., Chen, D., 2020. Abrupt shift to hotter and drier climate over inner East Asia beyond the tipping point. Science 370 (6520), 1095–1099. https://doi.org/10.1126/science.abb3368.

Zhang, Z., Fan, B., Song, C., Zhang, X., Zhao, Q., Ye, B., 2023. Advances in root system architecture: functionality, plasticity, and research methods. J. Resour. Ecol. 14 (1), 15–24. https://doi.org/10.5814/j.issn.1674-764x.2023.01.002.

Zhu, S., Olde, L., Lewis, K., Quaife, T., Cardenas, L., Loick, N., Xu, J., Hill, T., 2023. Eddy covariance fluxes over managed ecosystems extrapolated to field scales at fine spatial resolutions. Agric. For. Meteorol. 342, 109675. https://doi.org/10.1016/J.AGRFORMET.2023.109675.